

**ISPRS Journal of Photogrammetry and Remote Sensing**  
**On the consistency and stability of vegetation biophysical variables retrievals from**  
**Landsat-8/9 and Sentinel-2**  
--Manuscript Draft--

<b>Manuscript Number:</b>	PHOTO-D-24-01726
<b>Article Type:</b>	Research Paper
<b>Section/Category:</b>	Optical remote sensing
<b>Keywords:</b>	Validation; Landsat; Sentinel-2; LAI; fAPAR; canopy cover
<b>Corresponding Author:</b>	Najib Djamai, Ph.D. Natural Resources Canada Ottawa, ON CANADA
<b>First Author:</b>	Najib Djamai, Ph.D.
<b>Order of Authors:</b>	Najib Djamai, Ph.D. Richard Fernandes Lixin Sun Gang Hong Luck A. Brown Harry Morris Jadu Dash
<b>Abstract:</b>	Systematic decametric resolution global mapping of vegetation biophysical variables, including fraction of absorbed photosynthetically active radiation (fAPAR), fraction of vegetation cover (fCOVER), and leaf area index (LAI), is required to support various activities, including climate adaptation, crop management, biodiversity monitoring, and ecosystem assessments. The Canada Centre for Remote Sensing (CCRS) version of the Simplified Level 2 Prototype Processor (SL2P-CCRS) enables global mapping of these variables using freely available medium resolution multispectral satellite data from Sentinel-2 (S2) and Landsat-8/9 (LS) data. In this study, fiducial reference measurements (RMs) from the National Ecological Observatory Network (NEON) supplemented with regional measurements from CCRS were used to evaluate the consistency between SL2P-CCRS estimates of fAPAR, fCOVER and LAI from LS and S2 data and to quantify their temporal stability. SL2P-CCRS estimates of fCOVER (Accuracy (A)~0.03, Uncertainty (U)~0.13) and fAPAR (A~0.03, U~0.13) from LS and S2 were unbiased and generally similar based on 6569 LS-RMs and 4932 S2-RMs matchups. However, LAI estimates, especially for woody wetlands, deciduous forest, and mixed forest, were underestimated, with better estimates obtained using S2 (A~0.33, U~0.98) than LS (A~0.43, U~1.13). For all variables, SL2P-CCRS estimates from LS typically underestimated corresponding S2 estimates by between 10% and 20% but by up to 35% for LAI over broadleaf and mixed forests. The stability of SL2P-CCRS estimates from both LS and S2 fell within the Global Climate Observing System (GCOS) requirements with the mean (standard deviation) values of -0.01 yr-1 (0.06 yr-1) for LS LAI, 0.02 yr-1 (0.09 yr-1) for S2 LAI, and 0 yr-1 (0.01 yr-1) for fCOVER and fAPAR from both LS and S2.

**Djamai Najib, Ph.D.**  
Remote Sensing Physical Scientist

SPI/CCMEO/CCRS  
Natural Resources Canada  
580 Booth Street, Ottawa, ON, Canada K1A 0E4  
Email: [najib.djamai@nrcan-rncan.gc.ca](mailto:najib.djamai@nrcan-rncan.gc.ca)  
Phone: 01 819 620 2809

August 22nd, 2024

**Editor-in-Chief**  
ISPRS Journal of Photogrammetry and Remote Sensing

Dear Editor-in-Chief,

I am pleased to submit the manuscript titled "**On the consistency and stability of vegetation biophysical variables retrievals from Landsat-8/9 and Sentinel-2**" for consideration for publication in the ISPRS Journal of Photogrammetry and Remote Sensing. In this study, the Canada Centre for Remote Sensing (CCRS) version of the Simplified Level 2 Prototype Processor (SL2P-CCRS) was used to estimate three vegetation biophysical variables: fraction of absorbed photosynthetically active radiation (fAPAR), fraction of vegetation cover (fCOVER), and leaf area index (LAI) from both Sentinel-2 (S2) and Landsat-8/9 (LS) data. Fiducial reference measurements from the National Ecological Observatory Network (NEON), supplemented with regional measurements from CCRS, were utilized to evaluate the consistency between estimates of fAPAR, fCOVER, and LAI from LS and S2 data, as well as to quantify their temporal stability.

We believe that our findings provide novel insights into the use of multispectral satellite data from different medium-resolution sensors for mapping and monitoring vegetation cover, and will be of significant interest to the readers of the journal. Additionally, our study addresses the Committee of Earth Observation Satellite requirement to publish good practices for validating the performance of systematic global vegetation maps in terms of their ability to satisfy users requirements such as those of the Global Climate Observing System.

The research described in this paper has not been published previously and is not under consideration for publication elsewhere. All co-authors have contributed to the work and have approved the final version of the manuscript. We have followed the ethical guidelines set forth by the journal and have disclosed any potential conflicts of interest.

We hope that you find our manuscript suitable for the journal and we look forward to your feedback. Thank you for considering our submission. Please do not hesitate to contact me if you require any further information.

Thank you for your time and consideration.

Sincerely,  
Najib Djamai  
Remote Sensing Physical Scientist  
SPI/CCMEO/CCRS  
Natural Resources Canada  
580 Booth Street, Ottawa, ON, Canada K1A 0E4  
Email: [najib.djamai@nrcan-rncan.gc.ca](mailto:najib.djamai@nrcan-rncan.gc.ca)  
Phone: 01 819 620 2809

1   **On the consistency and stability of vegetation biophysical variables retrievals from Landsat-8/9 and**  
2   **Sentinel-2**

3   Najib Djamal<sup>1</sup>, Richard Fernandes<sup>1</sup>, Lixin Sun<sup>1</sup>, Gang Hong<sup>1</sup>, Luke A. Brown<sup>2</sup>, Harry Morris<sup>3</sup>, Jadu Dash<sup>4</sup>

4   <sup>1</sup> *Canada Centre for Remote Sensing, Natural Resources Canada, Ottawa, ON, K1A 0E4, Canada*

5   <sup>2</sup> *School of Science, Engineering and Environment, University of Salford, Manchester, United Kingdom*

6   <sup>3</sup> *Climate and Earth Observation Group, National Physical Laboratory, Teddington, United Kingdom*

7   <sup>4</sup> *School of Geography and Environmental Science, University of Southampton, Southampton, United  
8   Kingdom*

9

10   **Abstract**

11   Systematic decametric resolution global mapping of vegetation biophysical variables, including fraction of  
12   absorbed photosynthetically active radiation (fAPAR), fraction of vegetation cover (fCOVER), and leaf area  
13   index (LAI), is required to support various activities, including climate adaptation, crop management,  
14   biodiversity monitoring, and ecosystem assessments. The Canada Centre for Remote Sensing (CCRS)  
15   version of the Simplified Level 2 Prototype Processor (SL2P-CCRS) enables global mapping of these  
16   variables using freely available medium resolution multispectral satellite data from Sentinel-2 (S2) and  
17   Landsat-8/9 (LS) data. In this study, fiducial reference measurements (RMs) from the National Ecological  
18   Observatory Network (NEON) supplemented with regional measurements from CCRS were used to  
19   evaluate the consistency between SL2P-CCRS estimates of fAPAR, fCOVER and LAI from LS and S2 data and  
20   to quantify their temporal stability. SL2P-CCRS estimates of fCOVER (Accuracy (A)~0.03, Uncertainty  
21   (U)~0.13) and fAPAR (A~-0.03, U~0.13) from LS and S2 were unbiased and generally similar based on 6569  
22   LS-RMs and 4932 S2-RMs matchups. However, LAI estimates, especially for woody wetlands, deciduous  
23   forest, and mixed forest, were underestimated, with better estimates obtained using S2 (A~-0.33, U~0.98)  
24   than LS (A~-0.43, U~1.13). For all variables, SL2P-CCRS estimates from LS typically underestimated  
25   corresponding S2 estimates by between 10% and 20% but by up to 35% for LAI over broadleaf and mixed  
26   forests. The stability of SL2P-CCRS estimates from both LS and S2 fell within the Global Climate Observing  
27   System (GCOS) requirements with the mean (standard deviation) values of  $-0.01 \text{ yr}^{-1}$  ( $0.06 \text{ yr}^{-1}$ ) for LS LAI,  
28    $0.02 \text{ yr}^{-1}$  ( $0.09 \text{ yr}^{-1}$ ) for S2 LAI, and  $0 \text{ yr}^{-1}$  ( $0.01 \text{ yr}^{-1}$ ) for fCOVER and fAPAR from both LS and S2.

29   **Keywords:** Validation, Landsat, Sentinel-2, LAI, fAPAR, canopy cover

30        **1. Introduction**

31        Systematic global mapping of vegetation biophysical variables, including fraction of absorbed  
32        photosynthetically active radiation (fAPAR) , fraction of vegetation cover (fCOVER), and leaf area index  
33        (LAI), is required at decametric resolution to support climate adaptation, crop management, biodiversity  
34        monitoring, and ecosystem assessments (see Table ; WMO, 2022; Group on Earth Observation Global  
35        Agricultural Monitoring, 2023; Group on Earth Observation Biodiversity Observation Network, 2023).  
36        Satellite data records (SDRs) of multispectral imagery are primary inputs for algorithms capable of  
37        mapping these variables globally (WGClimate, 2017). Currently, only the Sentinel-2A and Sentinel-2B (S2)  
38        and Landsat 8 and Landsat 9 (LS) imagers offer systematic global coverage of such SDRs at decametric  
39        resolution in a free and open manner (European Space Agency, 2013; Gascon et al., 2017; United States  
40        Geological Survey, 2019; United States Geological Survey, 2022).

41

42        Biophysical variables maps derived from LS and S2 imagery have attained Committee on Earth Observation  
43        Satellites (CEOS) Validation Stage 3 (<https://lpvs.gsfc.nasa.gov/>) based on comparisons to fiducial  
44        reference measurements (RMs) at significant number of locations and time periods representative of  
45        global conditions (Fang et al., 2019; Ganguly et al., 2012; Kang et al., 2021; Brown et al., 2021a; Fernandes  
46        et al., 2023; Fernandes et al., 2024a; Amin et al., 2021). CEOS Stage 4 validation requires: i. quantification  
47        of the temporal stability of product accuracy, defined as the change in bias at interannual time scales, to  
48        derive long term trends and anomalies; and ii. the consistency between S2 and LS based products to satisfy  
49        the ≤10-day temporal resolution requirement of Global Climate Observing System (GCOS). CEOS Stage 4  
50        validation of S2 and LS fAPAR, fCOVER and LAI products has not yet been achieved due to the limited  
51        temporal overlap of SDRs and RMs. Recently available multi-annual RMs representative of North American  
52        biomes, coincident with S2 and LS SDRs, opened possibilities for Stage 4 validation of vegetation products  
53        over North America (Brown et al., 2020a; Fernandes et al., 2024b).

54

55        Several globally applicable algorithms are available for mapping biophysical variables from LS and S2 bi-  
56        directional surface reflectance (reflectance,  $\rho$ ) SDRs (Ganguly et al., 2012; Weiss and Baret, 2016; Pipia et  
57        al., 2021; Fernandes et al., 2024a; Wan et al., 2024). These algorithms use either look-up-table or  
58        regression estimators, both calibrated using either canopy radiative transfer models (RTMs), other  
59        products, or empirical databases (Baret and Buis, 2008; Fang et al., 2019; Ma and Liang, 2022). In this

60 study, we consider algorithms calibrated using RTMs since the same code and priors can be applied to  
61 both S2 and LS SDRs with minor changes in sensor specifications (Weiss and Baret, 2020), and since they  
62 are widely used for mapping coarse resolution vegetation variables products (Lacaze et al., 2015; Yan et  
63 al., 2016; Disney et al., 2018; Yan et al., 2018; Fang et al., 2019).

64

65 RTMs represent vegetation using either spatially homogeneous or spatially heterogeneous patterns  
66 (Widlowski et al., 2007). Numerical and empirical studies indicate that heterogeneous RTMs are required  
67 for unbiased LAI estimation over shrubs and forests (Myneni et al., 1997; Shabanov et al., 2005; Gonsamo  
68 et al., 2014; Brown et al., 2019; Fernandes et al., 2024a). The Landsat equivalent of the MODIS fAPAR/LAI  
69 algorithm (Ganguly et al., 2012) and the Canada Centre for Remote Sensing (CCRS) version of the S2  
70 Simplified Level 2 Prototype Processor (S2LP-CCRS, Fernandes et al., 2024a) use heterogeneous RTMs. This  
71 study validates SL2P-CCRS since its free and open code allows it to be recalibrated and applied to both LS  
72 and S2.

73

74 For a given sensor, SL2P-CCRS uses four land cover specific neural network regression algorithms to  
75 estimate a given biophysical variable: needleleaf forest (NF), broadleaf forest (BF), mixed forest (MF) and  
76 other land cover classes (OTHER). NF and BF algorithms are calibrated using simulations produced by  
77 applying sensor specific spectral response functions to database of 1nm resolution  $\rho$  simulated by the  
78 4SAIL2 heterogeneous RTM (Verhoef and Bach 2007) sampled with representative priors calibrated with  
79 field measurements available prior to 2024 and nominal sensor acquisition geometry (Fernandes et al.  
80 2024a). Previously, SL2P-CCRS used the average of the NF and BF algorithm estimates for MF. In this study,  
81 the MF algorithm is updated to use the same neural network architecture as the BF algorithm but a  
82 calibration database using 4SAIL2 simulations with input parameters sampled from the union of the BF  
83 and NF priors. The OTHER class is mapped using the SL2P algorithm (Weiss and Baret, 2016) based on the  
84 4SAIL homogeneous RTM (Verhoef, 1985) with priors corresponding to global in-situ measurements  
85 available prior to 2016.

86

87 For this study, SL2P-CCRS regressions were recalibrated for LS using a calibration database produced by  
88 applying LS spectral response functions ([https://landsat.gsfc.nasa.gov/satellites/landsat-8/spacecraft-  
instruments/operational-land-imager/spectral-response-of-the-operational-land-imager-in-band-band](https://landsat.gsfc.nasa.gov/satellites/landsat-8/spacecraft-instruments/operational-land-imager/spectral-response-of-the-operational-land-imager-in-band-band)-

90 [average-relative-spectral-response/](#)) to a database of 1nm resolution p simulated using the sampling  
91 scheme, same RTM and priors as used for S2 but with uniform sampling of LS acquisition geometry .  
92 Identical priors and RTMs were used to increase the consistency between LS and S2 estimates, to the  
93 extent the algorithms are not overly sensitive to differences in spectral sampling, acquisition geometry,  
94 and spatial resolution. Nevertheless, studies using regression algorithms calibrated with SAILH model  
95 suggest LS retrievals could have greater uncertainty than coincident S2 retrievals for canopies with high  
96 LAI values due to the absence of equivalent S2 red-edge bands with LS data (Djamai et al., 2018; Dong et  
97 al., 2023). As such, it is essential to quantify the relative uncertainty and bias between S2 and LS  
98 vegetation variables estimates to facilitate characterization of seasonal vegetation dynamics and long-  
99 term vegetation trends.

100

101 CEOS recommends using both comparison to RMs (validation) and comparison of products  
102 (intercomparison) to quantify the thematic performance of different combinations of mapping algorithms  
103 and SDRs (Fernandes et al., 2014). Validation allows one to quantify whether the likelihood products would  
104 satisfy user requirements and to identify systematic limitations due to SDRs or algorithms. In this study,  
105 SL2P-CCRS S2 and LS retrievals are validated over the same sites, although with different temporal  
106 sampling, to address both tasks. Intercomparison is also conducted over the validation sites to determine  
107 if the validation results are also reflected in between-product differences. CEOS has not previously  
108 identified methods for quantifying the temporal stability of vegetation variables estimates from products.  
109 Thus, statistics corresponding to both the expected value and confidence interval of stability are derived  
110 for fAPAR, fCOVER and LAI products here for the first time.

111

112 Our study addressed two questions based on the performed validation and intercomparison:

- 113 1. How do SL2P-CCRS fAPAR, fCOVER, and LAI estimates from LS compare to estimates from S2 in  
114 terms of accuracy (A), precision (P) and uncertainty (U) with respect to RMs and in terms of  
115 product intercomparison?
- 116 2. What is the stability (S) of products estimates from LS and S2 over North American sites with  
117 sufficient RMs temporal samples?

118

119 We hypothesized that:

120        1. LS fAPAR and fCOVER will be similar to corresponding S2 estimates and have similar A, P, U but LS  
 121              LAI will show a larger negative bias and greater uncertainty compared to S2 due to LS having no  
 122              red-edge bands.

123        2. Both LS and S2 will show much lower S (i.e. better) than retrieval uncertainty since stability is less  
 124              sensitive to local biases due to RTM error or uncertainties in specification of priors required for  
 125              RTM inversion.

126

127        The study scope was limited to vegetated North American sites, where multi-annual sampling of RMs were  
 128              available for numerous sites. The scope was further limited in that S2 SDRs only spanned 2019 to 2023  
 129              due to the absence of recently processed S2 Collection 1 SDRs on the Google Earth Engine (GEE) platform  
 130              on which SL2P-CCRS is currently deployed. Even so, our study included the largest validation dataset  
 131              applied to simultaneously validate LS and S2 fAPAR, fCOVER and LAI over North America to date.

132

133        Our study is novel in that, i. it is the first study to provide a Stage 4 validation of a globally applicable system  
 134              for mapping both vegetation variables from S2 and LS SDRs, ii. it presents a first quantification of stability  
 135              of derived products, and iii. it quantifies the consistency of S2 and LS based products using a representative  
 136              sample of matchups. We expect that users will gain a better understanding of the thematic performance  
 137              of both LS and S2 products from SL2P-CCRS, especially with respect to time series stability over regions  
 138              representative of our validation sites. Our findings will also provide algorithm producers a better  
 139              understanding of conditions under which improvements are needed to satisfy user requirements, as well  
 140              as a characterization of a baseline mapping system (SL2P-CCRS) for benchmarking new algorithms. Finally,  
 141              the methods presented will contribute to improve good practice for product validation.

142

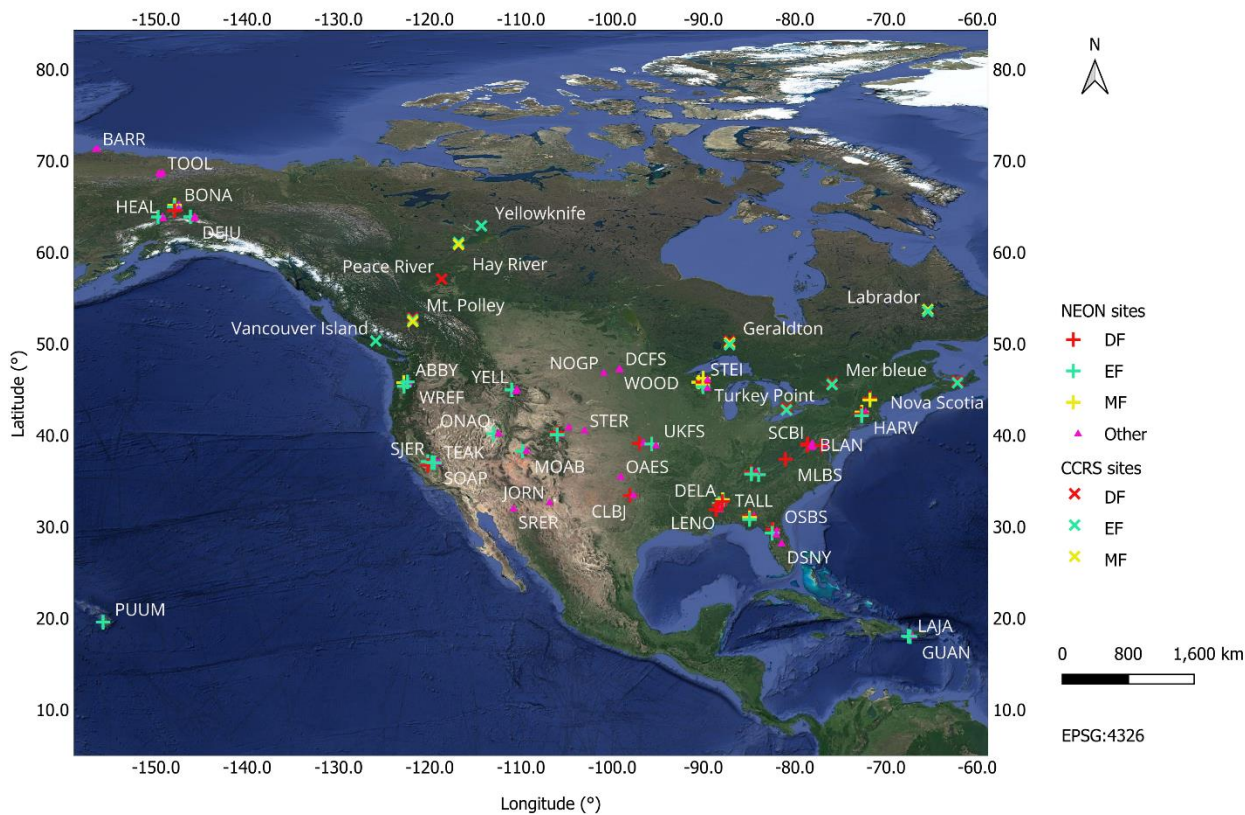
143        *Table 1. Vegetation biophysical variables definitions and GCOS threshold thematic user requirements.  
 144              Uncertainty corresponds to maximum of the absolute difference between the estimate and reference value  
 145              as a percentage of the reference measurement and the absolute difference between the estimate and  
 146              measurement value. Stability corresponds to the change in bias per year assuming fAPAR $\in [0,1]$  and  
 147              LAI $\in [0,10]$ .*

Acronym	Variable	Definition	GCOS requirements	
			Uncertainty	Stability

fAPAR	Fraction of absorbed Photosynthetically Active Radiation (PAR)	Fraction of PAR effectively absorbed by plants (for direct sun illumination)	max (10%, 0.05)	0.03 yr <sup>-1</sup>
fCOVER	Fraction of green vegetation cover	Green vegetation cover per unit horizontal ground area	max (10%, 0.05)	N/A
LAI	Leaf area index	Half the total green foliage area per unit horizontal ground area	max (20%, 0.5)	0.06 yr <sup>-1</sup>

148 **2. Materials and methods**149 **2.1. Materials**150 **a. Reference measurements**

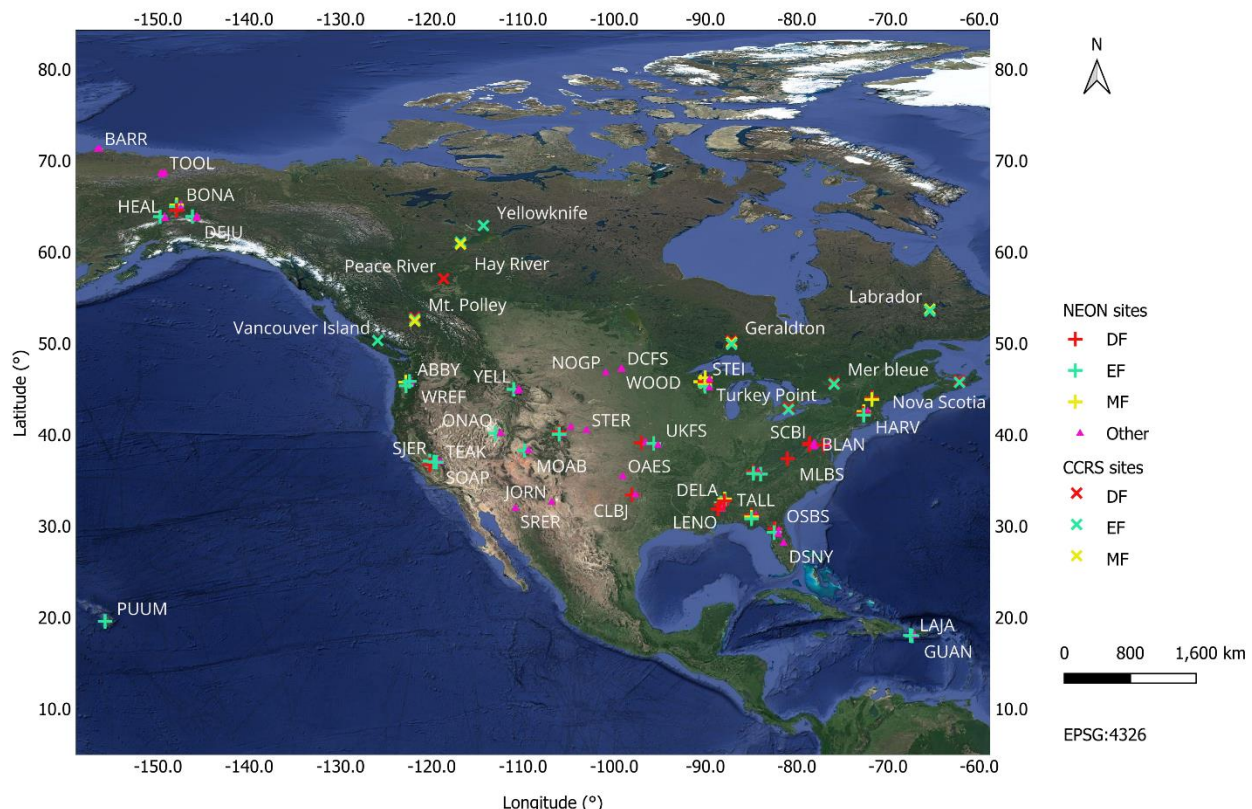
151 RMs were acquired at 47 National Ecological Observatory Network (NEON,

152 <https://data.neonscience.org/data-products/>) and 10 CCRS sites across North America (

153

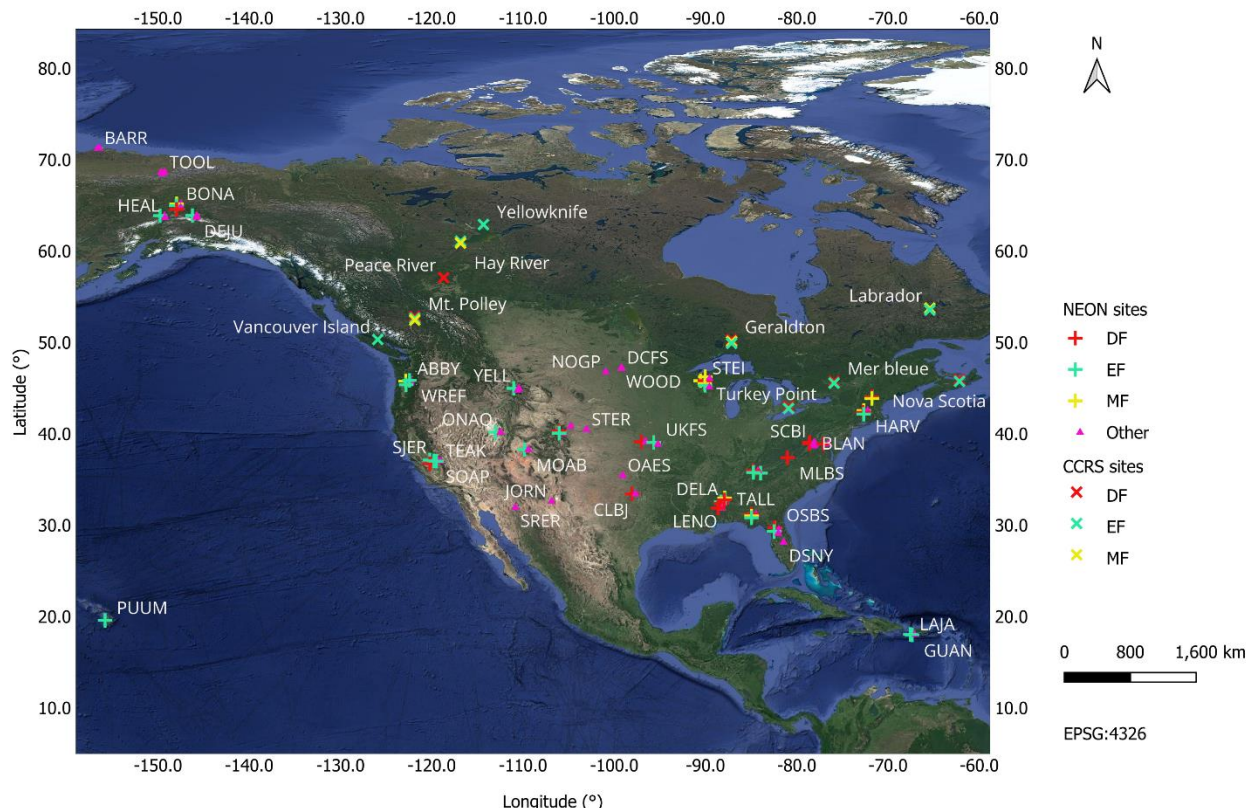
154 Figure 1; Table A1 in Appendix A). These 57 sites corresponding to 47 sites used for previous S2  
 155 validation studies (Brown et al., 2021b; Fernandes et al., 2023; Fernandes et al., 2024a) and 10  
 156 additional NEON sites. NEON sites are representative of 20 North American ecoclimatic domains and

157 span 11 United States of America National Land Cover Database classes (NLCD,  
 158 <https://www.usgs.gov/centers/eros/science/national-land-cover-database>) (Table 1). A total of 1074  
 159 elementary sampling units (ESUs) were visited across the NEON sites during the growing seasons of 2013  
 160 through 2022. For each NEON site, a minimum of three ESUs were sampled bi-weekly during the growing  
 161 season at each NEON site and the remainder were sampled near peak season. Additionally, 48 EF, 7 DF,  
 162 and 9 MF ESUs were measured across the CCRS sites; with each ESU sampled once during July and  
 163 August between 2019 and 2020. For both NEON and CCRS, fAPAR, fCOVER, and LAI RMs were  
 164 simultaneously measured at each ESU on each sampling date.) and 10 CCRS sites across North America (



165  
 166 Figure 1; Table A1 in Appendix A). These 57 sites corresponding to 47 sites used for previous S2  
 167 validation studies (Brown et al., 2021b; Fernandes et al., 2023; Fernandes et al., 2024a) and 10  
 168 additional NEON sites. NEON sites are representative of 20 North American ecoclimatic domains and  
 169 span 11 United States of America National Land Cover Database classes (NLCD,  
 170 <https://www.usgs.gov/centers/eros/science/national-land-cover-database>) (Table 1). A total of 1074  
 171 elementary sampling units (ESUs) were visited across the NEON sites during the growing seasons of 2013  
 172 through 2022. For each NEON site, a minimum of three ESUs were sampled bi-weekly during the growing  
 173 season at each NEON site and the remainder were sampled near peak season. Additionally, 48 EF, 7 DF,

174 and 9 MF ESUs were measured across the CCRS sites; with each ESU sampled once during July and  
 175 August between 2019 and 2020. For both NEON and CCRS, fAPAR, fCOVER, and LAI RMs were  
 176 simultaneously measured at each ESU on each sampling date.



177  
 178 Figure 1. NEON and CCRS sites across North America. Symbols indicate dominant NLCD forest class or  
 179 otherwise.

180 *Table 1. NEON and CCRS ESUs and RMs by NLCD land cover class (forested classes are in bold). SL2P-CCRS*  
 181 *algorithm is indicated for each class.*

NLCD land cover class (Abbrev.)	SL2P-CCRS Groupings of NLCD classes	NEON		CCRS	
		#ESUs	#RM	#ESUs	#RMs
<b>Evergreen forest (EF)</b>	NF	263	3427	9	48
<b>Deciduous forest (DF)</b>	BF	249	3923	5	7
<b>Mixed forest (MF)</b>	MF	49	639	3	9
<b>Woody wetland (WW)</b>	BF	88	326	0	0
Cultivated crops (CC)	OTHER	50	702	0	0
Emergent herbaceous wetland (EHW)	OTHER	19	79	0	0
Grassland herbaceous (GH)	OTHER	165	2101	0	0
Pasture hay (PH)	OTHER	32	934	0	0
Sedge herbaceous (SH)	OTHER	20	126	0	0

Shrub scrub (SS)	OTHER	139	1704	0	0
Total		1074	13961	17	64

182

183 RMs were derived from in-situ digital hemispherical photographs (DHPs), processed using free and open-  
 184 access software packages, corrected for biases due to woody material using empirical or site-specific  
 185 calibration, and characterized in terms of uncertainty using fiducial reference measurements for  
 186 vegetation protocols. These approaches are documented in previous studies (Brown et al., 2021a;  
 187 Fernandes et al., 2023; Fernandes et al., 2024a), so only details relevant to the current study are given  
 188 below.

189

190 DHPs were measured within a 20m square for the NEON sites and 15m x 35m rectangle for the CCRS  
 191 sites, centred on each ESU using a cross-sampling design for the NEON sites and two parallel 35m long  
 192 transects for the CCRS sites. For each date, co-located upward and downward looking DHPs were  
 193 sampled at ~1m height at 12 locations for the NEON sites and 14 locations for the CCRS sites, spaced  
 194 evenly along the sampled cross or line transects. NEON DHPs were acquired using 36.3-megapixel Nikon  
 195 D810 or D800 cameras (<https://www.nikonusa.com/p/d810/1542/overview>) with a Nikon 16 mm  
 196 Fisheye lens (<https://en.nikon.ca/p/af-fisheye-nikkor-16mm-f28d/1910/overview>). CCRS DHPs were  
 197 acquired using 45.7-megapixel Nikon D850 cameras (<https://en.nikon.ca/p/d850/1585/overview>) with a  
 198 Nikon 8 mm Fisheye lens (<https://en.nikon.ca/p/af-s-fisheye-nikkor-8-15mm-f35-45e-ed/20066/overview>). Both NEON and CCRS DHPs corresponded a 180° diagonal field of view. DHP  
 200 images were visually quality controlled and, for CCRS, enhanced using Nikon ViewNX-I  
 201 ([https://en.nikon.ca/p/viewnx-i/ViewNX\\_i/overview](https://en.nikon.ca/p/viewnx-i/ViewNX_i/overview)) to improve visual separation of canopy versus soil  
 202 or sky. Only regions in images within 60° of nadir were processed to constrain the spatial footprint of  
 203 measurements and minimize RM uncertainty due to camera tilt. Subsequently, the spatial support of  
 204 downward measurements fell within the nominal ESU boundary while the spatial support of upward  
 205 measurements was a circle centred on the ESU with diameter ~1.5 times the canopy height (Fernandes  
 206 et al. 2023).

207

208 HemiPy (Brown et al., 2023) and CAN-EYE V6.45 (<https://can-eye.paca.hub.inrae.fr>) were respectively used  
209 to estimate the fraction of woody and green cover per horizontal ground area (fCANOPY), the fraction of  
210 PAR intercepted by woody and green elements (fIPAR), and plant area index (PAI) defined as half of the  
211 total vegetation surface area per unit horizontal ground area at the NEON and CCRS sites. PAI was  
212 corrected for clumping using the approach of Lang and Yueqin (1986) corresponding to an expected bias  
213 of ~-5% and upper bound on bias of ~-10% (Fernandes et al., 2024a). RMs uncertainty was quantified as  
214 described in Fernandes et al. (2023) and Brown et al. (2021b).

215

216 Coefficients corresponding to the woody-to-total area ratio were applied to relate fCANOPY, fIPAR, and PAI  
217 to fCOVER, fAPAR, and LAI (Table B1 in Appendix B). For canopies with a height less than 19m, coefficients  
218 were estimated from values based on destructive sampling at sites with the same land cover class (Brown  
219 et al., 2021a). ESU specific coefficients were derived for NEON overstory canopies with >=19m tall using  
220 CAN-EYE as qualitative assessment of DHPs showed far greater woody area than expected based on  
221 woody-to-total area ratios for shorter canopies with the same land cover. For these NEON ESUs, CANEYE  
222 was first applied to DHP imagery to estimate PAI and then applied once more to the DHP imagery,  
223 enhanced using View-NXi ([https://fr.nikon.ca/p/viewnx-i/ViewNX\\_i/overview](https://fr.nikon.ca/p/viewnx-i/ViewNX_i/overview)) to highlight green pixels, to  
224 estimate LAI (Appendix C, Table C1). This approach required manual labelling of substantial portions of  
225 imagery, so it was not feasible to apply for LAI estimation for all sites. This approach has not been validated  
226 for NEON ESUs so an uncertainty of 0.19 for the ratio of woody-to-total area is assumed based on  
227 validation of a similar approach using HemiPy over a broadleaf forest (Brown et al. 2021b). ESU fAPAR,  
228 fCOVER, and LAI RM estimates and their uncertainties were derived by a weighted sum of corresponding  
229 overstory, and understory measurements described in Brown et al. (2021a).

230 b. Satellite data

231 GEE LS Level-2 (L2) LANDSAT/LC08/C02/T1\_L2 ([https://developers.google.com/earth-](https://developers.google.com/earth-engine/datasets/catalog/LANDSAT_LC08_C02_T1_L2)  
232 [engine/datasets/catalog/LANDSAT\\_LC08\\_C02\\_T1\\_L2](https://developers.google.com/earth-engine/datasets/catalog/LANDSAT_LC08_C02_T1_L2)), LANDSAT/LC09/C02/T1\_L2  
233 ([https://developers.google.com/earth-engine/datasets/catalog/LANDSAT\\_LC09\\_C02\\_T1\\_L2](https://developers.google.com/earth-engine/datasets/catalog/LANDSAT_LC09_C02_T1_L2)) and S2  
234 Level-2A (L2A) ([https://developers.google.com/earth-](https://developers.google.com/earth-engine/datasets/catalog/COPERNICUS_S2_SR_HARMONIZED)  
235 [engine/datasets/catalog/COPERNICUS\\_S2\\_SR\\_HARMONIZED](https://developers.google.com/earth-engine/datasets/catalog/COPERNICUS_S2_SR_HARMONIZED)) p products were used as input to SL2P-  
236 CCRS. These data are reformatted versions of original USGS products (for LS) and European Space Agency  
237 (for S2) Level 2 p products.

238

239 LS L2 products include  $\rho$  gridded at 15m resolution for one panchromatic band and 30m resolution for  
 240 nine bands within the shortwave spectrum (Table ) derived from Operational Land Imager (Knight et al.,  
 241 2014, Levy et al., 2024) measurements of top-of-atmosphere radiance using the Landsat Surface  
 242 Reflectance Code (Vermote et al., 2018), in addition to the acquisition geometry, and a mask indicating  
 243 clear sky land pixels based on the fMASK4.0 algorithm (Qiu et al., 2019). LS L2 products have a  
 244 geolocation uncertainty of <13m 90% circular error probable (CEP; Storey et al., 2014) and a radiometric  
 245 uncertainty of  $\sim 0.05\rho + 0.005$  for flat terrain (Doxani et al., 2018). fMASK 4.0 has a clear sky omission  
 246 error of 4.8% and commission error of 4.6% (Qiu et al., 2019).

247

248 S2 L2A products include  $\rho$  gridded at 10m resolution for four bands, 20m resolution for six bands and  
 249 60m resolution for three bands derived from Multispectral Instrument (Drusch et al., 2012)  
 250 measurements of top-of-atmosphere radiance using Sen2Cor Version 2.4.0 (Müller-Wilm et al., 2017,  
 251 Table 4), as well as the mean acquisition geometry for the product granule and a gridded 20m resolution  
 252 scene classification map indicating clear sky land pixels. S2 L2A products have a geolocation uncertainty  
 253 <12.5m 95% CEP (Gascon et al., 2017) and a radiometric uncertainty of  $\sim 0.05\rho + 0.005$  for flat terrain  
 254 (Djamai and Fernandes, 2018; Doxani et al., 2018). Sen2Cor has a clear sky omission error of 3% and  
 255 commission error of 6% (European Space Agency, 2020). For each L2A product, the matching S2Cloudless  
 256 cloud probability product (Zupanc, 2017) was used to reduce clear sky commission errors. L2A product  
 257 pixels were flagged as cloudy if the S2Cloudless cloud probability was greater than 50%.

258

259 *Table 3. LS bands (SL2P-CCRS input bands are in bold)*

Band	Resolution (m)	Central Wavelength (nm)	Description
B1	30	443	Coastal / Aerosol
B2	30	482	Blue
<b>B3</b>	<b>30</b>	<b>562</b>	<b>Green</b>
<b>B4</b>	<b>30</b>	<b>655</b>	<b>Red</b>
<b>B5</b>	<b>30</b>	<b>865</b>	<b>Near-Infrared</b>
<b>B6</b>	<b>30</b>	<b>1610</b>	<b>Short Wave Infrared</b>
<b>B7</b>	<b>30</b>	<b>2200</b>	<b>Short Wave Infrared</b>
B8	15	590	Panchromatic
B9	30	1375	Cirrus

260 *Table 4. S2 bands (SL2P-CCRS input bands are in bold)*

Band	Resolution (m)	Central Wavelength (nm)	Description
B1	60	443	Coastal / Aerosol
B2	10	490	Blue
<b>B3</b>	<b>10</b>	<b>560</b>	<b>Green</b>
<b>B4</b>	<b>10</b>	<b>665</b>	<b>Red</b>
<b>B5</b>	<b>20</b>	<b>705</b>	<b>Vegetation red edge</b>
<b>B6</b>	<b>20</b>	<b>740</b>	<b>Vegetation red edge</b>
<b>B7</b>	<b>20</b>	<b>783</b>	<b>Vegetation red edge</b>
B8	10	842	Near-Infrared
<b>B8a</b>	<b>20</b>	<b>865</b>	<b>Near-Infrared</b>
B9	60	940	Water vapour
B10	60	1375	Cirrus
<b>B11</b>	<b>20</b>	<b>1610</b>	<b>Short Wave Infrared</b>
<b>B12</b>	<b>20</b>	<b>2190</b>	<b>Short Wave Infrared (SWIR)</b>

261 c. Land Cover

262 The 30m resolution circa 2020 North America Land Cover Monitoring System (NALCMS) land cover map  
 263 was used to determine the SL2P-CCRS regression algorithm applied to each S2 or LS pixel (Table 2). The  
 264 thematic error of NALCMS product has been assessed over Canada with 79.9% correct labelling for all 18  
 265 classes and 83% correct labelling of forest classes (Latifovic et al., 2012). NALCMS products matched the  
 266 nominal LS sampling grid, so resampling was not required when using SL2P-CCRS with LS SDRs. Nearest  
 267 neighbour resampling was used to assign NALCMS land cover to 20m S2 pixels. Additional uncertainty in  
 268 SL2P-CCRS S2 retrievals due to resampling was negligible as ESUs were located within patches of  
 269 undisturbed homogeneous land covers (Brown et al., 2020a; Fernandes et al., 2023) and the SL2P-CCRS  
 270 RTM land cover classes were highly generalized.

271 2.2. Methods

272 a. NEON RMs Quality Control

273 NEON RMs were subjected to additional quality control since HemiPy, in contrast to CANEYE, is completely  
 274 automated. For each variable, a moving window temporal filtering was applied to measurements at each  
 275 ESU to identify spurious RMs. The  $i^{th}$  RM ( $RM_i$ ) with associated uncertainty  $\widetilde{RM}_i$ , was flagged as spurious  
 276 if the three following conditions held simultaneously:

$$277 |RM_i - RM_l| > \max(\widetilde{RM}_i, \varepsilon_V) \quad (1)$$

$$278 |RM_i - RM_r| > \max(\widetilde{RM}_i, \varepsilon_V) \quad (2)$$

279  $(RM_i - RM_l) \cdot (RM_i - RM_r) > 0$  (3)

280 where  $RM_l$  and  $RM_r$  are respectively the previous and the next RMs acquired within +/-15 days and  $\varepsilon_V$  is  
 281 an empirical land cover specific threshold (e.g. Figure C1 in Appendix BC). Only 0.31% of LAI, 0.97% of  
 282 fCOVER, and 0.93% of fAPAR RMs were flagged and removed from validation (Table C1 in Appendix BC).

283

284 b. Correcting NEON RMs estimates for ESUs with moss.

285

286 Exploratory data analysis identified a constant SL2P-CCRS bias of ~0.9 for LAI, ~0.25 for fAPAR, and ~0.25  
 287 for fCOVER for RMs from Alaskan tundra sedge sites (BARR, TOOL, and DEJU) for both LS and S2 (Figure C1  
 288 in Appendix C). These sites had only downward DHPs as overstory vegetation was absent. Examination of  
 289 DHPs indicated virtually 100% moss cover that had been labelled by HemiPy as non-vegetated area. Moss  
 290 canopy LAI values range from 1 to over 20, with significant between species differences (Niinemets and  
 291 Tobias, 2019). Moss canopy LAI is inversely correlated with leaf thickness so the functional role of moss  
 292 LAI in controlling carbon and water fluxes differs from vascular plants (Zotz and Kahler, 2007). For example,  
 293 Niinemets and Tobias (2019) noted that “for acrocarpous moss *T. ruralis*, already the upper 2mm of canopy  
 294 reduces the light level to only 20% of incident light”. This suggests that moss LAI cannot be considered  
 295 directly when validating satellite LAI products since the high LAI values are accompanied by extremely thin  
 296 foliage with different functional and structural characteristics to vascular vegetation. At the same time, a  
 297 method is required to characterize the ability of satellite products to track vascular LAI at mossy sites.  
 298 Keeping in mind the limitation to vascular LAI, RMs for all mossy ESUs were increased by the observed bias  
 299 between all satellite products and RMs matchups, irrespective of sensor. Land cover specific thematic  
 300 metrics were reported to isolate this class should our approach be refined by future studies.

301

302 c. Estimation of LS and S2 vegetation variables

303

304 The Landscape Evolution and Forecasting (LEAF; Fernandes et al. 2021) was used to extract LS and S2 L2A  
 305 clear sky land pixels whose centroid fell within 30m of an ESU centroid, for S2, and 45m, for LS, of an ESU  
 306 centroid and within  $\pm 7$  days of a RM. The nearest NALCMS land cover pixel was associated with each  
 307 sampled S2 and LS reflectance.

308

309 A Python implementation of SL2P-CCRS (<https://github.com/djmainajib/SL2P-SL2PCCRS PYTHON>),  
 310 identical to that implemented in the GEE code for LEAF, was applied to each sampled measurement.  
 311 SL2P-CCRS uses separate land cover specific neural networks, using  $p$  measured for a LS or S2 pixel (Table  
 312 3 for LS and Table 4 for S2) together with available acquisition geometry, to estimate each variable.  
 313 Additionally, SL2P-CCRS flags measurement whose  $p$  does not lie within +/-0.05 of RTM simulations used  
 314 for calibration or if the estimate falls outside the range of variable values within the simulations. The  
 315 neural network calibration for NF and BF is described in Fernandes et al. (2024a) while the calibration for  
 316 OTHER is described in Fernandes et al. (2023). The neural network calibration for MF was identical to  
 317 that of BF but with priors corresponding to the union of NF and BF priors. These neural network  
 318 regression algorithms correspond to groupings of NLCD classes (Table 2).

319  
 320 For each biophysical variable, the trimmed median residual between a given RM and matching SL2P-CCRS  
 321 estimates was computed for S2 and LS products. Trimming corresponded to discarding residuals exceeding  
 322 the 90%ile for a given RM. It was applied since perfect spatial matching and clear sky identification was  
 323 not possible for the large sample size used in our study, and it did not result in changes in statistical tests  
 324 of differences in performance between sensors or estimates of stability but improved the  
 325 representativeness of the measurement error modelled when fitting conditional A, P, U curves.

326  
 327 d. Validation and intercomparison  
 328 Following good practice (Fernandes et al., 2014) scatter plots as well as the population A, U, coefficient of  
 329 determination ( $R^2$ ), and uncertainty agreement ratio (UAR) were computed separately for LS and S2  
 330 products for all matchups and for each NLCD class based on the following equations.

$$331 \quad A = \frac{1}{N} \sum_{i=1}^N (\hat{y}_i - y_i) \quad (4)$$

$$332 \quad U = \sqrt{\frac{1}{N} \sum_{i=1}^N (\hat{y}_i - y_i)^2} \quad (5)$$

$$333 \quad P = \sqrt{\frac{1}{N} \sum_{i=1}^N (\hat{y}_i - y_i - A)^2} \quad (6)$$

$$334 \quad R^2 = \left[ \frac{\sum_{i=1}^N (\hat{y}_i - \bar{y})(y_i - \bar{y})}{\sum_{i=1}^N (\hat{y}_i - \bar{y})^2 \cdot (y_i - \bar{y})^2} \right]^2 \quad (7)$$

$$335 \quad UAR = \frac{1}{N} \sum_{i=1}^N I \left( \left| \frac{\hat{y}_i - y_i}{y_i} \right| \leq \varepsilon_{rel} \cup |\hat{y}_i - y_i| \leq \varepsilon_{max} \right) \quad (8)$$

336 where,  $\hat{y}_i$ ,  $y_i$  are respectively the SL2P-CCRS estimate and RM for the  $i^{th}$  of  $N$  comparisons,  $\bar{y}$ ,  $\bar{\hat{y}}$  are their  
337 corresponding average values,  $\varepsilon_{rel}$ ,  $\varepsilon_{max}$  are respectively the relative and maximum target uncertainty  
338 requirement, and  $I$  is the indicator function.

339

340 Good practice also requires quantifying the A, P and U conditional on a given RM value to reduce the  
341 impact of the sampling distribution of RMs on validation results and to isolate problematic retrieval  
342 conditions (Fernandes et al., 2014). Ideally, one would have sufficient samples to produce conditional A, P  
343 and U curves for each NLCD class. Due to the imbalanced nature of RMs sampling within a given NLCD  
344 class, conditional A, P, U curves were fitted for RMs grouped as either forested or non-forested ESUs. *Figure*  
345 This partitioning was useful since SL2P-CCRS assumes a homogenous canopy for non-forested classes and  
346 a heterogeneous canopy for forested classes (Fernandes et al., 2024a). For each group and sensor, A and  
347 U, conditional on either the RM (producer validation) or the product estimates (user validation), were  
348 estimated by fitting third order polynomial weighted least squares regressions to residuals and absolute  
349 residuals as described in Fernandes et al. (2023). Weights corresponded to the Euclidean sum of the  
350 standard error of sampled product estimates and the RM one standard deviation. P, conditional on the  
351 RM, was estimated by fitting third order polynomial weighted least squares regressions to absolute  
352 residuals after first subtracting the modelled conditional A.

353

354 Intercomparison was performed using all clear sky S2 and LS  $\rho$  data between April and September  
355 inclusively for 3x3 pixels centred on each ESU whose dates matched within +/-1 day. SL2P-CCRS was  
356 applied to each sampled measurement to produce estimates of fAPAR, fCOVER, and LAI. Following good  
357 practice, kernel density plots of matchups for groupings of NLCD classes corresponding to SL2P-CCRS  
358 neural network regression algorithms, and, given the fact there were sufficient intercomparisons samples  
359 for each NLCD class, NLCD class specific A and U statistics were derived.

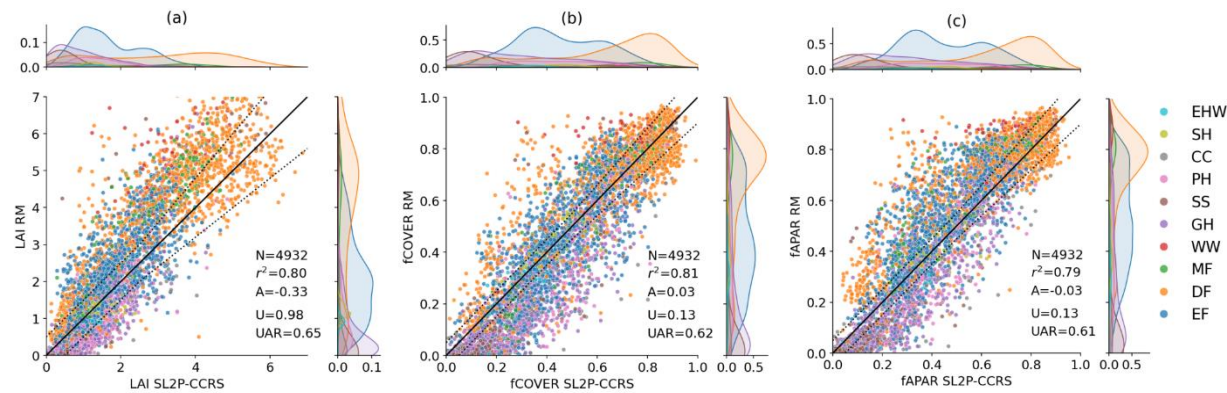
360

361 At each site, for each NLCD class present, S was estimated as the slope of the ordinary least squares  
362 regression of the average annual bias of ESUs corresponding to that NLCD class (see Figure E1 in Appendix  
363 E). The 95% confidence interval of the regression slope was used as the precision of estimated S. Only  
364 results for sites with at least 5 years for LS, or 4 years for S2, due to the shorter input records, with at least  
365 5 inter-annual samples per year were reported.

366

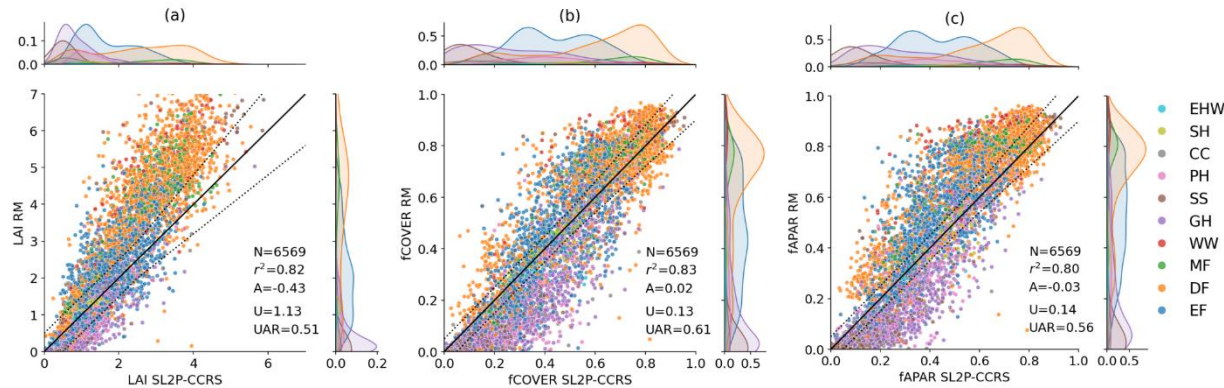
367 **3. Results**368 **3.1. Validation**

369 A total of 4932 S2-RM matchups (Figure ) and 6569 LS-RM (Figure 3) matchups were used during  
 370 validation. The RMs range of LAI, fCOVER, and fAPAR matchups are, respectively, [0.0, 6.87], [0, 0.99], and  
 371 [0, 0.95] for S2, and [0.02, 5.88], [0, 0.96], and [0, 0.93] for LS. RM histograms were qualitatively similar  
 372 between sensors although LS had a slightly greater relative frequency of extreme values. However, RMs  
 373 histograms differed between NLCD land cover, with forest classes dominating values above the 50%ile for  
 374 each variable. For fCOVER and fAPAR, S2 and LS  $R^2$ , A, U and UAR for all matchups were virtually identical  
 375 at respectively ~0.8, ~0.03, ~0.13 and ~0.60. However, for LAI, A, U, and UAR were better for S2  
 376 (respectively, 0.33, 0.98, and 0.65) compared to LS (respectively, 0.43, 1.13, and 0.51).



377

378 *Figure 2.* Scatter plots of SL2P-CCRS estimates of LAI (a), fCOVER (b), and fAPAR (c) obtained from S2 data  
 379 versus matching RMs together with population validation metrics. Dashed lines bound target user  
 380 requirement around solid 1:1 line. Colours corresponds to NLCD land cover class.

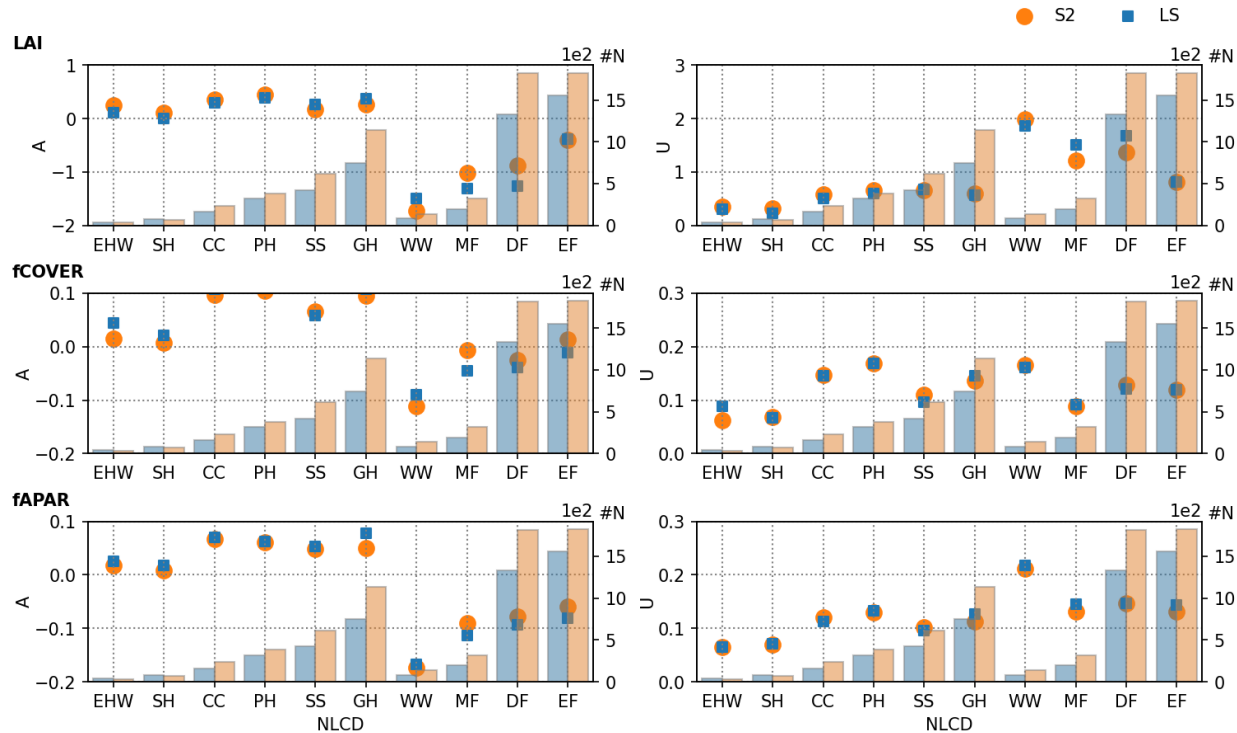


381

382 *Figure 3.* Scatter plots of SL2P-CCRS estimates of LAI (a), fCOVER (b) and fAPAR (c) obtained from LS data  
383 versus matching RMs together with population validation metrics. Dashed lines bound target user  
384 requirement around solid 1:1 line. Colours corresponds to NLCD land cover class.

385

386 The of matchups by land cover class were comparable between S2 and LS (Figure ) with the most  
387 matchups over the EF and DF forest classes primarily due to the considerable number of ESUs for these  
388 classes (Table 1). EHW and SH had the least matchups, ranging between 35 and 79 depending on sensor  
389 and NLCD class (Tables D1 and D2 in Appendix D). Between sensors, difference in metrics were, in most  
390 cases, smaller than the between land cover differences, with the largest between sensor A (U) difference  
391 of ~0.4 (~0.32) for LAI observed for DF, ~0.04 (~0.03) for fCOVER observed for MF and EHW, and ~0.03  
392 (~0.02) for fAPAR observed for MF and GH. However, substantial differences in A and U were observed  
393 between forested and non-forested classes. In terms of accuracy, forested classes were underestimated  
394 by between ~0.05 and ~2 for LAI and between ~0.05 and ~0.20 for fAPAR while non-forested classes  
395 were slightly overestimated by ~0.5 for LAI and ~ 0.1 for fAPAR (Figure ). fCOVER was also slightly  
396 overestimated for non-forest classes but was almost unbiased for forest classes. LAI U ranged between  
397 ~0.2 and ~0.7 for non-forested classes and between ~0.8 and ~2 for forested classes. However, fCOVER  
398 and fAPAR U, both ranging between ~0.05 and 0.20, did not show systematic forest/non-forest trends,  
399 indicating that the accuracy error contributes more to U for LAI than fAPAR and fCOVER.



400  
401  
402

Figure 4. NLCD class specific A and U validation statistics for SL2P-CCRS estimates of LAI, fCOVER, and fAPAR obtained from LS and S2 data together with match-up sample size N (histograms).

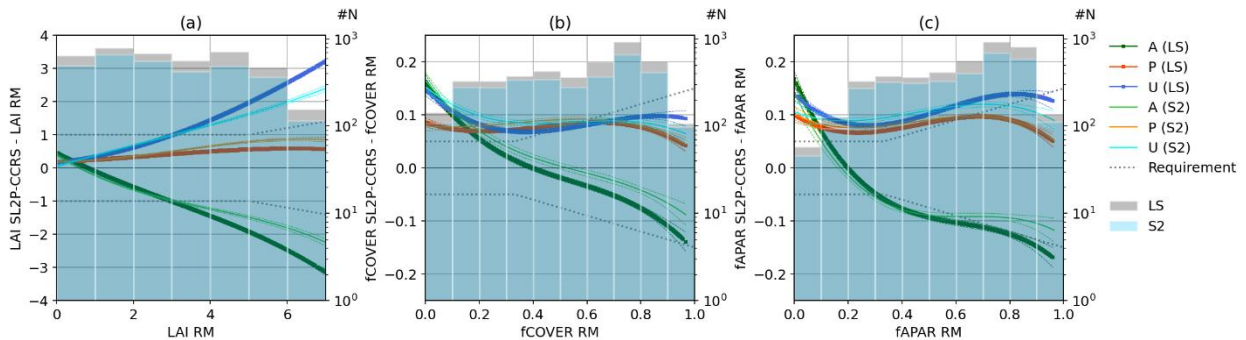
403

404 Conditional A, P, U curves were generally monotonic for forested classes except for extreme fCOVER and  
405 fAPAR values where sampling was limited (Figure ). For LS, LAI A tended quasi-linearly from ~0.5 at LAI 0  
406 to ~-3 at LAI 6, while both fCOVER and fAPAR A tended monotonically from ~0.15 at very low values to ~-  
407 0.15 at the highest values. LS P was almost constant across the range of each variable at ~0.5 for LAI, ~0.08  
408 fCOVER, and ~0.09 for fAPAR. As a result, LS LAI U increased from ~0.1 at LAI 0 to ~3 at LAI 7. LS fCOVER  
409 and fAPAR U was typically ~0.1 but increased to ~0.15 at extremely low values due to a positive bias. S2  
410 LAI A was similar to LS for LAI<3 but showed a proportional improvement over LS for LAI>3, with an A of  
411 ~-2 at LAI 7 versus ~-3 for LS. The improvement in A for S2 versus LS combined with similar P for both  
412 sensors translated into a modest improvement in S2 U compared to LS for LAI>3 but only minor differences  
413 for LAI<3. fCOVER and fAPAR A were slightly better for S2 versus LS above fCOVER>0.5 and fAPAR>0.7,  
414 respectively, but otherwise no significant between-sensor differences were observed for these variables.

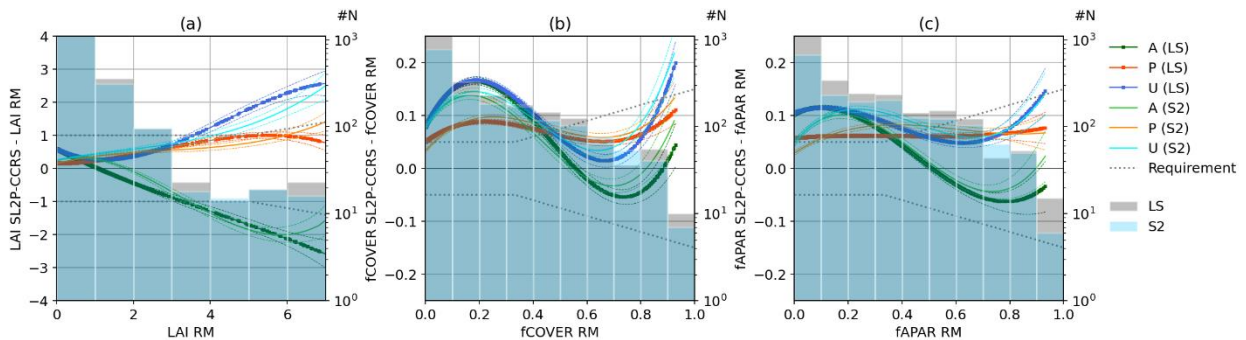
415

416 Conditional A, P, U curves for non-forested classes were quasi-monotonic for LAI, with only slight  
417 improvements for S2 versus LS at LAI>4 and fCOVER or fAPAR >0.7 (Figure 6). For both S2 and LS, LAI A

418 showed a similar trend as observed for forests, but with underestimation reaching ~-2.5 rather than ~-3  
 419 at LAI 7. Precision error was ~0 at LAI 0 and gradually increased to ~1 at LAI 5. As a result, LAI U increased  
 420 gradually with LAI reaching ~2.5 at LAI 7. P for fCOVER and fAPAR was almost constant at ~0.8 and ~0.6,  
 421 respectively. However, sinusoidal A and U curves were observed for fCOVER with overestimation below  
 422 0.5 and underestimation for larger values. Additionally, a positive inflection in U was observed for  
 423 fCOVER and fAPAR >0.9 but this is likely due to insufficient samples to constrain the 3<sup>rd</sup> order polynomial  
 424 fit.



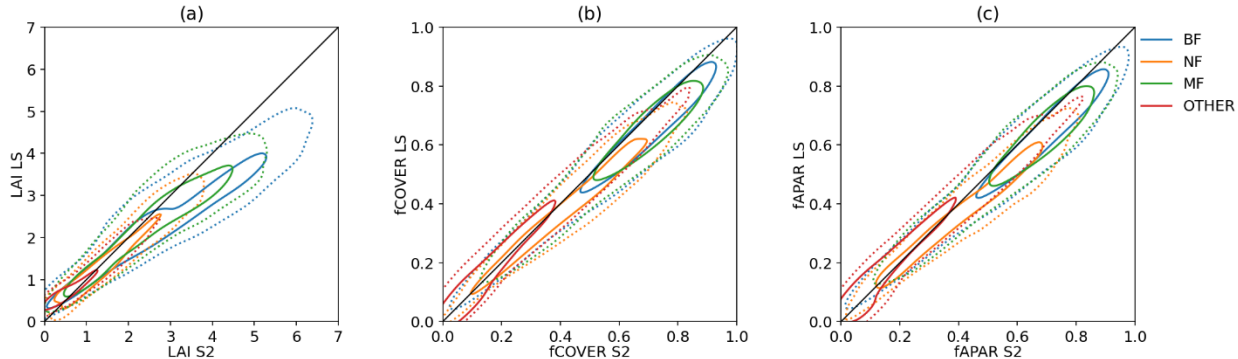
425  
 426 *Figure 5. APU curves and the corresponding 95% confidence intervals (dashed contours) for SL2P-CCRS*  
 427 *estimates of LAI (a), fCOVER (b) and fAPAR (c) obtained from forested classes compared to APU*  
 428 *curves for the corresponding estimates from S2. Dashed grey lines bound target user requirements.*



429  
 430 *Figure 6. APU curves and the corresponding 95% confidence intervals (dashed contours) for SL2P-CCRS*  
 431 *estimates of LAI (a), fCOVER (b) and fAPAR (c) obtained from non-forested classes compared to APU*  
 432 *curves for the corresponding estimates from S2. Dashed grey lines bound target user requirements.*

## 433 3.2. Intercomparison

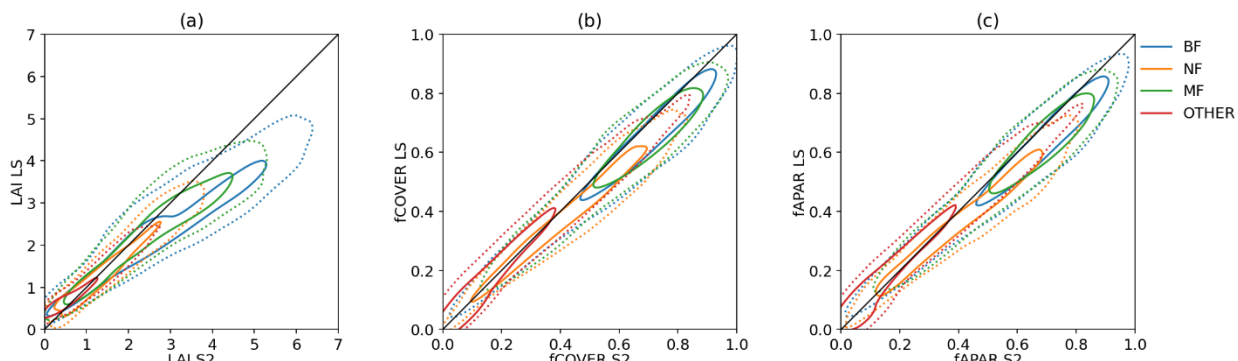
434 Intercomparison resulted in ~11800 NF, ~13200 BF, ~2000 MF and ~19000 OTHER matchups for each  
 435 variable (



436

437 Figure , Table E1 in Appendix E). For fCOVER and fAPAR, LS and S2 retrievals agreed within 0.15 at 50%ile  
 438 and 0.20 at 10%ile irrespective of land cover, with S2 estimates slightly higher than matching LS estimates  
 439 (linear regression slope of ~0.88).

440 LAI intercomparisons, in contrast to fAPAR and fCOVER, were different between NF and OTHER classes  
 441 versus BF and MF classes. For NF and OTHER, LAI agreed within 0.5 at 50%ile and 1 at 10%ile with a linear  
 442 regression slope of 0.82 for NF and 0.80 for OTHER, indicating S2 LAI was slightly higher than matching LS  
 443 LAI. In contrast, the linear regression slope of 0.62 for BF and 0.67 for MF indicated S2 LAI was consistently  
 444 larger than LS LAI.



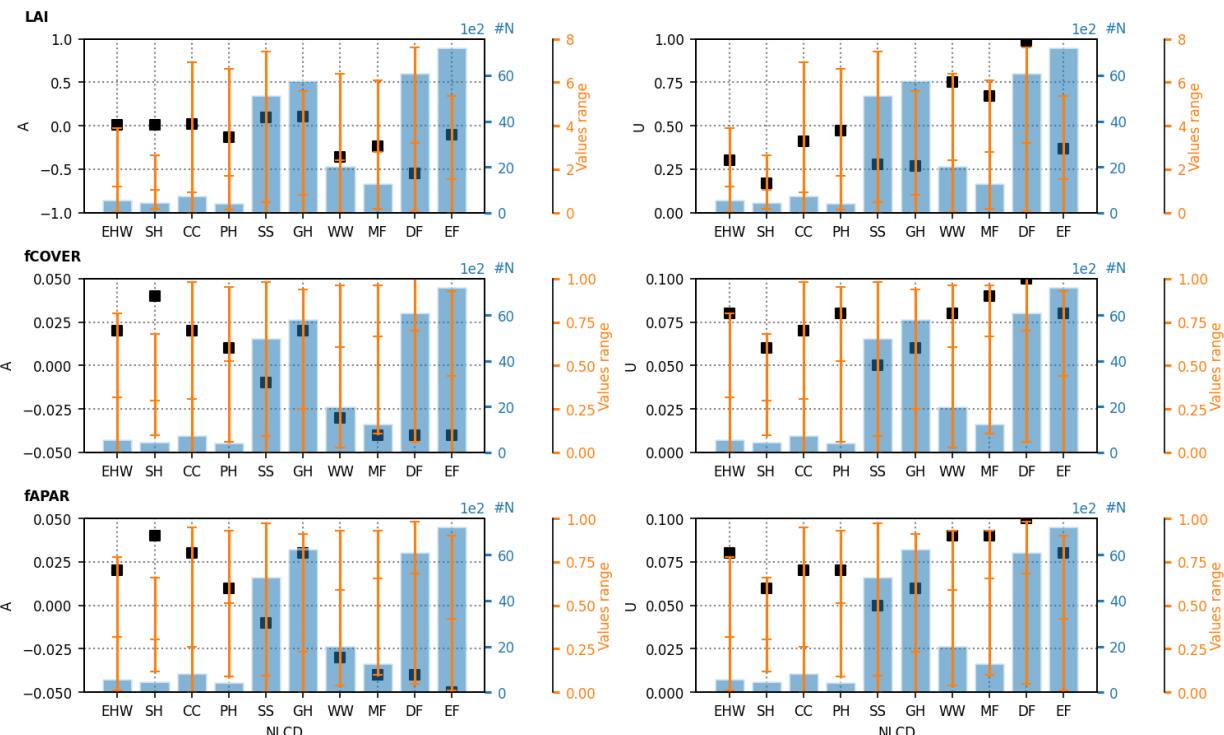
445

446 Figure 7. Density contour plots of SL2P-CCRS LAI (a), fCOVER (b) and fAPAR (c) estimates from LS data  
 447 compared to the corresponding estimates from S2 data (reference): continuous (dashed) lines present  
 448 50%ile (10%ile) and continuous black line present the 1:1 line.

449

450 The same metrics shown in Figure 4 were also computed for intercomparisons (Figure ) to determine the  
 451 relative magnitude of between-sensor differences versus differences between each sensor and RMs for  
 452 each NLCD class.

453 For LAI, intercomparison A was ~0 for non-forested and EF classes and ranged from ~-0.25 to ~-0.55 for  
 454 WW, MF, and DF classes. fAPAR and fCOVER intercomparison A were bimodal between non-forested and  
 455 forested classes, with a positive bias between 0.01 and 0.04 for the former (except for SS) and a negative  
 456 bias between -0.02 and -0.05 for the latter. These accuracy errors were generally less than 50% of the  
 457 corresponding validation A. This was expected since SL2P-CCRS RTMs and RTM priors are identical for S2  
 458 and LS. However, U was generally much larger than A, ranging from 0.18 to 1 for LAI and from 0.05 to 0.1  
 459 for fCOVER and fAPAR. Even so, intercomparison U for a given cover class was generally less than 75% of  
 460 the corresponding validation U for that class (compare Figures 4 and 8).



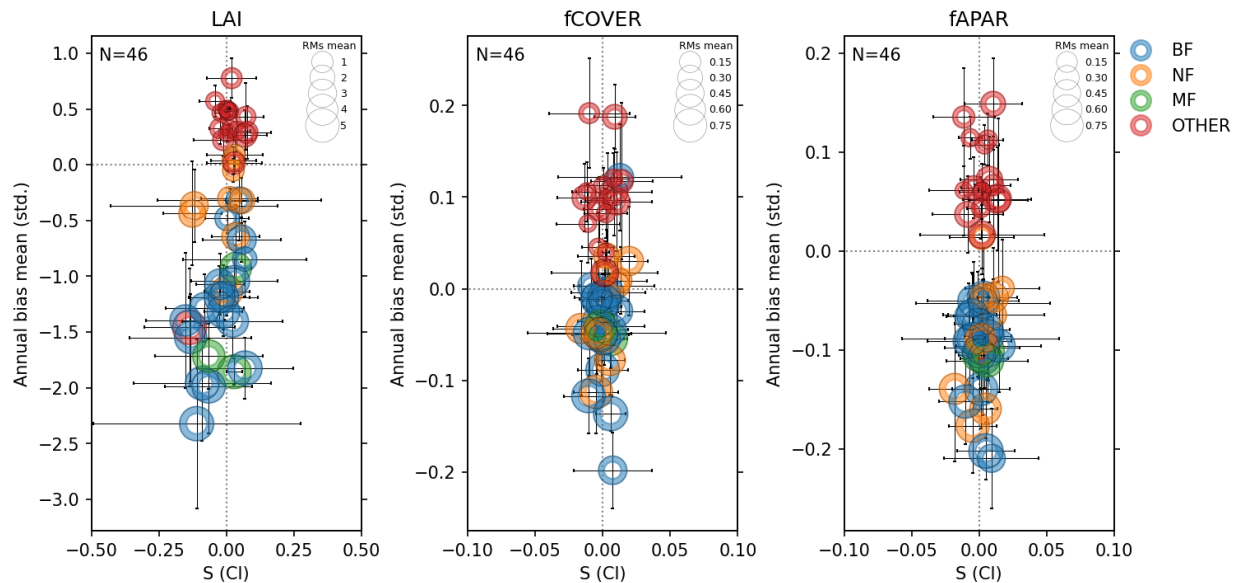
461  
 462 Figure 8. Class specific A and U statistics between SL2P-CCRS estimates of LAI, fCOVER, and fAPAR from LS  
 463 and the corresponding estimates from S2 (reference), together with the samples size (histogram) and the  
 464 variation range of estimates from S2 (bars) as a function of NLCS land cover class.

465

## 466      3.3. Stability

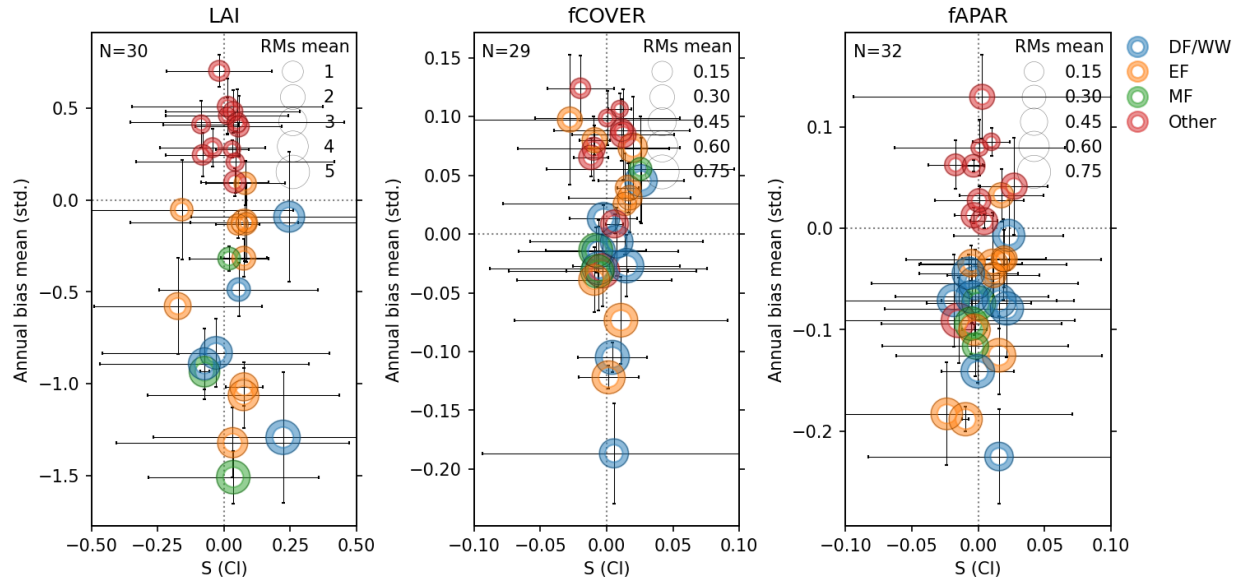
467      S was quantified for 46 sites for LS (Figure 9) and ~30 sites for S2 (Figure 2). LS S ranged from ~-0.15 yr<sup>-1</sup>  
 468      to 0.08 yr<sup>-1</sup> for LAI with a mean (standard deviation) across sites of -0.01 (0.06) yr<sup>-1</sup>, and from -0.02 yr<sup>-1</sup> to  
 469      0.02 yr<sup>-1</sup> for fCOVER and fAPAR with a mean (standard deviation) of 0 (0.01) yr<sup>-1</sup>. S2 S values ranged  
 470      between -0.17 yr<sup>-1</sup> and 0.25 yr<sup>-1</sup> for LAI with a mean (standard deviation) of 0.02 (0.09) yr<sup>-1</sup> and from -0.03  
 471      yr<sup>-1</sup> to 0.03 yr<sup>-1</sup> for fCOVER and fAPAR with a mean (standard deviation) of 0 (0.01) yr<sup>-1</sup>. LS S confidence  
 472      intervals ranged from 0.01 to 0.38 for LAI and from 0 to 0.06 for fAPAR and fCOVER. However, confidence  
 473      intervals for S2 S were ~3 times greater than LS S due to the shorter time span of S2 and RM matchups  
 474      versus LS and RM matchups.

475      LS S was weakly correlated with bias ( $R \sim 0.43$  for LAI,  $\sim 0.10$  for fCOVER, and  $\sim 0.06$  for fAPAR) and with the  
 476      site average RMs magnitude ( $R \sim -0.41$  for LAI,  $\sim -0.02$  for fCOVER, and  $\sim -0.03$  for fAPAR). Similarly, S2 S  
 477      was weakly correlated with bias ( $R \sim -0.13$  for LAI,  $\sim -0.06$  for fCOVER, and  $\sim 0.18$  for fAPAR) and with the  
 478      site average RMs magnitude ( $R \sim 0.22$  for LAI,  $\sim 0$  for fCOVER, and  $\sim -0.16$  for fAPAR) (Tables F1 and F2 in  
 479      Appendix F).



480

481      *Figure 9. Scatter plots of LS S versus annual bias mean for SL2P-CCRS estimates of LAI, fCOVER and fAPAR:*  
 482      *x error bars (S confidence interval), y error bars (annual bias standard deviation), circles size (RMs mean),*  
 483      *and color (groupings of NLCD classes).*



484

485 *Figure 2.* Scatter plots of S2 S versus annual bias mean for SL2P-CCRS estimates of LAI, fCOVER and fAPAR:  
 486 x error bars (S confidence interval), y error bars (annual bias standard deviation), circles size (RMs mean),  
 487 and color (groupings of NLCD classes).

488      **4. Discussion**

489 This study focussed on the thematic performance of SL2P-CCRS estimates, derived from four satellite  
490 imagers, for three biophysical vegetation variables, fAPAR, fCOVER, and LAI, related to vegetation status  
491 and function. These variables are useful both for modelling and monitoring applications but one cannot  
492 ignore the fact that spectral vegetation indices are also widely used for monitoring vegetation status and  
493 trends (Giovos et al., 2021; Gao et al. 2020; Ferchichi et al., 2022). Our study focused on vegetation  
494 biophysical variables, rather than spectral vegetation indices, as they can be easily validated and are thus  
495 well suited for quantifying trends and anomalies of vegetation properties.

496 Our use of reference measurements from in-situ networks (Brown et al., 2020a; Fernandes et al., 2024a)  
497 allowed us to incorporate the uncertainty of estimated residuals when computing validation statistics.  
498 These networks are being supplemented by new regional networks that leverage automated  
499 measurements and data processing (e.g. Brown et al., 2021a; Brown et al., 2023) but it is critical that they  
500 continue long term monitoring. This study extends our previous CEOS Level 3 validation of vegetation  
501 variables from S2 to LS and, for the first time for such products, quantifies time-dependent bias in terms  
502 of both inter-annual stability and biases that could arise when combining products from different sensors.  
503 Inter-annual stability is a fundamental requirement for use cases such as environmental accounting  
504 (Chraibi et al. 2022) and vegetation-climate studies that rely on trend analysis (Xi et al., 2022,  
505 <https://doi.org/10.1016/j.agrformet.2021.108704>) and for use cases, such as reclamation assessments,  
506 afforestation and reforestation assessment, and disturbance mapping that rely on anomalies (Rochdi et al.  
507 2014; Diniz et al., 2015; Hermosilla et al. 2019; Hird et al., 2021). Quantifying sensor dependent biases is  
508 required since currently, only a combination of LS and S2 imagers have the potential for meeting GCOS  
509 requirements for  $\leq 10$ -day products. Moreover, these biases highlight the potential degradation in product  
510 performance when using strategies such as harmonizing sensors to the lowest common spectral sampling  
511 (e.g. the Harmonized Landsat and Sentinel 2 products, Claverie et al., 2018).

512 Our study used perhaps the largest RMs dataset for simultaneous fCOVER, fAPAR, and LAI validation to  
513 date in terms of spatial and temporal sampling. here are other sources of fAPAR measurements but these  
514 are not yet qualified as fiducial reference measurements and often do not include understory values  
515 (Putzenlechner et al., 2019, 2020; Sanchez-Azofeifa, 2022). New automated imaging sensors may improve  
516 this situation (Brown et al., 2020b). At the same time, our RMs had limitations that impact the  
517 representativeness of our results and, to a lesser extent, their statistical confidence. The most significant  
518 limitation is that we did not sample sloped terrain or pixels with significant land cover mixtures that

519 products will generally also map, and that users may require information about. Both limitations can be  
520 partially addressed from the user perspective by flagging such areas in product metadata using ancillary  
521 information. The additional uncertainty due to mixed pixels can also be addressed using high spatial  
522 resolution reference maps as performed in Fernandes et al. (2024b) using the original SL2P algorithm.  
523 However, validation over sloped terrain requires new RMs that should be a priority for future networks.

524

525 We also identified two other limitations with the RMs. The first was the lack of representative woody-to-  
526 total area ratio estimates for forested sites not used in our previous work (Fernandes et al., 2023;  
527 Fernandes et al., 2024a). Visual assessment of DHPs for four forest sites with canopies >19m tall indicated  
528 tall and wide trunks with high relative crown base height (Appendix C). These were reprocessed using  
529 CANEYE twice to first estimate PAI and then LAI. Since this procedure required manual delineation of green  
530 vegetation cover, it was time consuming, requiring over an hour per plot, compared to the automated  
531 HemiPy PAI estimation. We used a woody-to-total area ratio uncertainty based on a single study that used  
532 HemiPy with green vegetation automatically identified from DHPs with both visible and near-infrared  
533 imagery (Brown et al., 2024). This uncertainty of 0.19 is ~twice that of 0.11 from destructive sampling but  
534 at the same time is likely less biased than the latter. More work is required to quantify the uncertainty of  
535 woody-to-total area ratio using our CANEYE approach specifically and for all approaches in general.

536

537 The second limitation was the constant bias observed for retrievals over sites with substantial moss cover.  
538 For fCOVER and fAPAR, this bias was due to the RMs not including moss cover. This is a limitation of HemiPy  
539 that could be addressed by CANEYE reprocessing. However, in the absence of a good practice for dealing  
540 with LAI validation over mosses, we adopted a pragmatic approach of removing the empirical bias by  
541 assuming the RM had a constant incorrect offset. This approach underestimates the potential bias and  
542 uncertainty of all products at these sites but does not detract from the goal of our study to quantify the  
543 consistency and stability of both LS and S2 products since the bias correction is constant. Moreover, this  
544 correction did not have a significant impact on either population, or conditional statistics given the fact it  
545 was limited to four sites.

546

547 Our study used land cover specific algorithms including a Python implementation  
548 (<https://github.com/djmainajib/SL2P-SL2PCCRS PYTHON>) of the Simplified Level 2 Prototype Processor

549 (Weiss and Baret, 2020) for S2 and LS over the OTHER class. The SNAP implementation of SL2P was not  
550 used as we have identified discrepancies with our implementation that we previously attributed to bugs  
551 in the original MATLAB code used to calibrate the SNAP neural networks (Fernandes et al., 2024a). We  
552 continue to see studies and applications using the SNAP solution and are concerned that this will both  
553 hamper community validation and result in potential errors in downstream use of products derived from  
554 SNAP. This can be addressed by open-source publication of the algorithms as is the case for SL2P-CCRS.

555 The sampling distributions of S2 and LS matchups were imbalanced between land cover classes but were  
556 similar between sensors within classes (Figure 2 versus Figure 3). This allows for comparison of conditional  
557 statistics between sensors without concern for sample dependent differences in metrics. fCOVER and  
558 fAPAR from LS and S2 are found unbiased and with virtually identical A $\sim$ 0.03, U $\sim$ 0.13, and UAR $\sim$ 0.60, while  
559 LAI was underestimated, with better estimates obtained with S2 (A $\sim$ -0.33, U $\sim$ 0.98, UAR $\sim$ 0.65) compared  
560 to LS (A $\sim$ -0.43, U $\sim$ 1.13, and UAR $\sim$ 0.51). For all variables, S2 and LS provided generally similar A, P, and U  
561 conditional on RMs although S2 LAI and fCOVER A error is  $\sim$ 10% lower than LS for LAI $>3$  and fCOVER $>0.5$   
562 (Figures 6 and 7). Similarity in S2 and LS A and U metrics is also observed on a land cover specific basis,  
563 again with S2 showing slightly better A and U for forests (Figure 4) which could be explained by their  
564 predominance for dense canopy samples (Figures 2 and 3).

565

566 Conditional S2 A, P, U curves were virtually identical to those reported in Fernandes et al. (2023) and  
567 Fernandes et al. (2024a) using subsets of the RMs with the same algorithms. This suggests that the RMs  
568 sample is sufficiently large and diverse so that further sampling has minimal impact conditional metrics.  
569 This is important both because it indicates our earlier and current samples are indeed representative of  
570 sampled biomes and terrain conditions and that we have achieved a Stage 4 validation that is only limited  
571 by the need for continued RMs. For all variables, validation metrics showed far greater sensitivity to land  
572 cover than sensor (Figure 4). Essentially, metrics differed systematically between forested and non-  
573 forested classes. For LAI, the non-forested classes were almost unbiased while the forested classes had a  
574 negative bias between -0.05 and -2 as also observed in Fernandes et al. (2024). Some of this difference  
575 may be due to the limited number of high LAI values for non-forested samples, but the conditional A and  
576 U for forest classes were also  $\sim$ 0.5 worse than the non-forest estimate for LAI $>5$ . Moreover, the systematic  
577 difference in biases persisted for fAPAR and fCOVER, although now they were approximately equal in  
578 magnitude but opposite in sign. These differences suggest that, unlike LAI, the fAPAR and fCOVER bias is  
579 not necessarily due to canopy heterogeneity as hypothesized in Fernandes et al. (2024a) since otherwise

580 we would expect unbiased estimates for non-forests. It may be that RMs are systematically biased since  
581 the same pattern was observed for fCOVER and fAPAR. One possibility is that the RMs protocol requires  
582 DHP positioned away from canopy elements by at least 2-3 times their width. For forests, this requires  
583 DHP points located away from trunks and hence within gaps. The fAPAR and fCOVER biases were small  
584 ~0.1 but important since they exceed the current GCOS requirement for U.

585 Intercomparisons results (Figure 7) were consistent with the corresponding validation results in terms of  
586 similarity for fCOVER and fAPAR retrievals between sensors, and LS showing a greater LAI underestimation  
587 than S2. These findings are also consistent with validation results with LS and S2 retrievals agreeing  
588 generally within the validation precision, except for LAI over MF, DF, and WW (Figure 7). For these classes,  
589 S2 LAI was substantially higher than LS LAI for LAI>3 (slope~0.6). The absence of a similar bias for EF may  
590 be due to the relatively low frequency of high LAI values for EF intercomparisons, but a lower  
591 underestimation is also obtained for EF LAI validation compared to WW, DF, and MF (Figure 4). Further,  
592 the larger sample size with inter-comparisons confirms that the validation result was not a sampling  
593 artifact. Considering the algorithms and matchup methods, the forest bias between S2 and LS supports  
594 the hypothesis that it is due to differences in spectral sampling. Indeed, the bias is not likely due to the  
595 input SDR processing chain since then it would have been seen with non-forested classes and less dense  
596 forests. It has long been noted that signal saturation of visible bands can result in low signal to noise ratios  
597 that in turn limit the range of retrieved high LAI values from inversion of RTMs (Myneni et al., 1997). While  
598 LS has SWIR bands that may alleviate this problem (Fernandes et al. 2023), SL2P-CCRS assumes identical  
599 multiplicative input noise and as such is likely still placing undue weight on the visible bands, specifically  
600 the red band of LS. S2, with red-edge bands, may not depend on the low signal to noise ratio for red band  
601 as noted by Dong et al. (2023). Indeed, Fernandes et al. (2024b) found the same saturation when using a  
602 retrieval algorithm based only on S2 10m bands that did not include red-edge or SWIR sampling. The  
603 systematic bias between S2 and LS could be corrected a posterior using matchups and could be applied to  
604 harmonized SDRs.

605 LS stability fell within GCOS requirements. This was not expected considering the precision error of all  
606 products. Indeed, the fCOVER stability of less than 0.02 yr-1 indicates one could detect changes of 0.2  
607 fCOVER per decade, well within the requirement of many systems for tracking reclamation, revegetation,  
608 and gradual vegetation cover loss. Granted the stability is based on annual average bias but this is  
609 necessary to remove the impact of seasonality or differences in the dates of intra-annual matchups.  
610 Comparisons to automated sensor networks can assess seasonal stability but would require a sufficient

611 temporal baseline not widely available currently. S2 stability was similar to LS on average although the  
612 range observed was larger due to the shorter S2 period examined. The confidence interval of S2 stability  
613 results could be improved by using new Collection 1 data that extends back to 2016.

614 **5. Conclusions**

615 This study evaluated the consistency and stability of SL2P-CCRS estimates of fAPAR, fCOVER and LAI from  
616 LS and S2 data over North American forested and non-forested sites. Fiducial RMs from NEON and regional  
617 CCRS sites are used.

618 Based on 4932 S2-RM comparisons and 6569 LS-RM comparisons, A and U of SL2P-CCRS estimates of  
619 fCOVER ( $A \sim 0.03$ ,  $U \sim 0.13$ ) and fAPAR ( $-A \sim 0.03$ ,  $U \sim 0.13$ ) from LS and S2 are similar. However, LAI estimates  
620 from S2 ( $A \sim -0.33$ ,  $U \sim 0.98$ ) are slightly better than estimates from LS ( $A \sim -0.43$ ,  $U \sim 1.13$ ); with the largest  
621 difference observed for LAI > 3 over woody wetlands, deciduous forest, and mixed forest. These results are  
622 confirmed by LS against S2 intercomparison showing that SL2P-CCRS estimates from LS and S2 agreed  
623 within 0.15 at 50%ile for fCOVER and fAPAR and within 0.5 at 50%ile for LAI, except for woody wetland,  
624 deciduous forest, and mixed forest, for which substantially lower estimates are generally obtained using  
625 LS compared to S2.

626 The stability of SL2P-CCRS estimates from LS and S2 fell within GCOS requirements with a mean (standard  
627 deviation) value over sites of  $-0.01 \text{ yr}^{-1}$  ( $0.06 \text{ yr}^{-1}$ ) for LS LAI,  $0.02 \text{ yr}^{-1}$  ( $0.09 \text{ yr}^{-1}$ ) for S2 LAI, and  $0 \text{ yr}^{-1}$  ( $0.01$   
628  $\text{yr}^{-1}$ ) for fCOVER and fAPAR from both LS and S2. However, the confidence intervals of S2 stability estimates  
629 often exceeded GCOS requirements due to the limited inter-annual overlap with RMs.

630 Our findings support the hypothesis that SL2P-CCRS LAI, fAPAR, and fCOVER products from LS and S2 can  
631 be combined to enhance temporal sampling, although sensor specific bias correction should be applied to  
632 LAI as recommended in Fernandes et al. 2023. Future studies should exploit these times series to monitor  
633 the status and trends of vegetation and to support models of crop productivity, land surface fluxes, and  
634 habitat.

635 **Acknowledgements**

636 We acknowledge Dr. Marie Weiss and Dr. Fred Baret for providing the original SL2P code that was used as  
637 a basis for the versions of SL2P-CCRS used in this study. We acknowledge the use of modified Sentinel 2  
638 data and derived products. This study has been undertaken using data from GBOV “Ground Based  
639 Observation for Validation” (<https://land.copernicus.eu/global/gbov>) funded by European Commission

640 Joint Research Centre FWC932059, part of the Global Component of the European Union's Copernicus  
641 Land Monitoring Service. We thank the National Ecological Observatory Network for the measurements  
642 collected in the field under the direction of Dr. Courtney Meier. We thank excellent reviewers and the  
643 editors of this paper. The work was funded by Natural Resources Canada's Earth Observation for  
644 Cumulative Effects Project.

645 **References**

- 646 Amin, E., Verrelst, J., Rivera-Caicedo, J.P., Pipia, L., Ruiz-Verdú, A., Moreno, J. (2021). Prototyping Sentinel-  
647 2 green LAI and brown LAI products for cropland monitoring. *Remote Sensing of Environment*, 255,  
648 112168, <https://doi.org/10.1016/j.rse.2020.112168>.
- 649 Baret, F., Buis, S. (2008). Estimating canopy characteristics from remote sensing observations: Review of  
650 methods and associated problems. In S. Liang (Ed.), *Advances in land remote sensing: System, modeling,*  
651 *inversion and application* (pp. 173-201), [https://doi.org/10.1007/978-1-4020-6450-0\\_7](https://doi.org/10.1007/978-1-4020-6450-0_7).
- 652 Brown, L. A., Ogutu, B. O., Dash, J. (2019). Estimating Forest Leaf Area Index and Canopy Chlorophyll  
653 Content with Sentinel-2: An Evaluation of Two Hybrid Retrieval Algorithms. *Remote Sensing*, 11(15), 1752,  
654 <https://doi.org/10.3390/rs11151752>.
- 655 Brown, L.A., Meier, C., Morris, H., Pastor-Guzman, J., Bai, G., Lerebourg, C., Gobron, N., Lanconelli, C.,  
656 Clerici, M., Dash, J. (2020a). Evaluation of global leaf area index and fraction of absorbed  
657 photosynthetically active radiation products over North America using Copernicus Ground Based  
658 Observations for Validation data. *Remote Sensing of Environment*, 247, 111935,  
659 <https://doi.org/10.1016/j.rse.2020.111935>.
- 660 Brown, L.A., Oguatu, B.O., Dash, J. (2020b). Tracking forest biophysical properties with automated digital  
661 repeat photography: A fisheye perspective using digital hemispherical photography from below the  
662 canopy. *Agricultural and Forest Meteorology*, 287, 107944,  
663 <https://doi.org/10.1016/j.agrformet.2020.107944>.
- 664 Brown, L.A. Fernandes, R., Djamai, N., Meier, C., Gobron, N., Morris, H., Canisius, F., Bai, G., Lerebourg, C.,  
665 Lanconelli, C., Clerici, M., Dash, J. (2021a). Validation of baseline and modified Sentinel-2 Level 2 Prototype  
666 Processor leaf area index retrievals over the United States. *ISPRS Journal of Photogrammetry and Remote*  
667 *Sensing*, 175, 71-87, <https://doi.org/10.1016/j.isprsjprs.2021.02.020>.
- 668 Brown, L., Camacho, F., García-Santos, V., Origo, N., Fuster, B., Morris, H., Pastor Guzman, J., Sanchez-  
669 Zapero, J., Morrone, R., Ryder, J., Nightingale, J., Boccia, V., Dash, J. (2021b). Fiducial reference  
670 measurements for vegetation bio-geophysical variables: an end-to-end uncertainty evaluation framework.  
671 *Remote Sensing*, 13(16), 3194, <https://doi.org/10.3390/rs13163194>.
- 672 Brown, L.A., Morris, H., Leblanc, S., Bai, G., Lanconelli, C., Gobron, N., Meier, C., Dash, J. (2023). HemiPy:  
673 a Python module for automated estimation of forest biophysical variables and uncertainties from digital  
674 hemispherical photographs. *Methods in Ecology and Evolution*, 14(12), 2329–2340,  
675 <https://doi.org/10.1111/2041-210X.14199>.

- 676 Brown, L.A., Morris, H., Morrone, R., Sinclair, M., Williams, O., Hunt, M., Bandopadhyay, S., Guo, X., Akcay, H., Dash, J. (2024). Near-infrared digital hemispherical photography enables correction of plant area index  
677 for woody material during leaf-on conditions. *Ecological Informatics*, 79, 102441,  
679 <https://doi.org/10.1016/j.ecoinf.2023.102441>.
- 680 Chraibi, E., De Boissieu, F., Barbier, N., Luque, S., Féret, J.B. (2022). Stability in time and consistency  
681 between atmospheric corrections: Assessing the reliability of Sentinel-2 products for biodiversity  
682 monitoring in tropical forests. *International Journal of Applied Earth Observation and Geoinformation*,  
683 112, 102884, <https://doi.org/10.1016/j.jag.2022.102884>.
- 684 Claverie, M., Ju, J., Masek, J. G., Dungan, J. L., Vermote, E. F., Roger, J.-C., Skakun, S. V., Justice, C. (2018).  
685 The Harmonized Landsat and Sentinel-2 surface reflectance data set. *Remote Sensing of Environment*,  
686 219, 145-161, <https://doi.org/10.1016/j.rse.2018.09.002>.
- 687 Diniz, C.G., de Almeida Souza, A.A., Santos, D.C., Dias, M.C., da Luz, N.C., de Moraes, D.R.V., Maia, J.S.,  
688 Gomes, A.R., da Silva Narvaes, I., Valeriano, D.M., Maurano, L.E.P., Adami, M. (2015). DETER-B: The new  
689 Amazon near real-time deforestation detection system. *IEEE Journal of Selected Topics in Applied Earth  
690 Observations and Remote Sensing*, 8(7), 3619-3628, <https://doi.org/10.1109/JSTARS.2015.2437075>.
- 691 Disney, M., Muller, J.-P., Kharbouche, S., Kaminski, T., Voßbeck, M., Lewis, P., Pinty, B. (2016). A new global  
692 fAPAR and LAI dataset derived from optimal albedo estimates: Comparison with MODIS products. *Remote  
693 Sensing*, 8(275), <https://doi.org/10.3390/rs8040275>.
- 694 Djamai, N., Fernandes, R. (2018). Comparison of SNAP-derived Sentinel-2A L2A product to ESA product  
695 over Europe. *Remote Sensing*, 10, 926, <https://doi.org/10.1016/j.rse.2019.03.020>.
- 696 Dong, T., Liu, J., Liu, J., He, L., Wang, R., Qian, B., McNairn, H., Powers, J., Shi, Y., Chen, J. M., Shang, J.  
697 (2023). Assessing the consistency of crop leaf area index derived from seasonal Sentinel-2 and Landsat 8  
698 imagery over Manitoba, Canada. *Agricultural and Forest Meteorology*, 109357,  
699 <https://doi.org/10.1016/j.agrformet.2023.109357>.
- 700 Doxani, G., Vermote, E., Roger, J. C., Gascon, F., Adriaensen, S., Frantz, D., Hagolle, O., Hollstein, A.,  
701 Kirches, G., Li, F., Louis, J., Mangin, A., Pahlevan, N., Pflug, B., Vanhellemont, Q. (2018). Atmospheric  
702 correction inter-comparison exercise. *Remote Sensing*, 10(2), 352, <https://doi.org/10.3390/rs10020352>.
- 703 Drusch, M., Del Bello, U., Carlier, S., Colin, O., Fernandez, V., Gascon, F., Hoersch, B., Isola, C., Laberinti,  
704 P., Martimort, P., Meygret, A., Spoto, F., Sy, O., Marchese, F., Bargellini, P. (2012). Sentinel-2: ESA's optical  
705 high-resolution mission for GMES operational services. *Remote Sensing of Environment*, 120, 25–36,  
706 <https://doi.org/10.1016/j.rse.2011.11.026>.
- 707 European Space Agency. (2013). *Sentinel-2: The operational Copernicus optical high resolution land  
708 mission*. Retrieved June 23, 2024, from <https://www.esa.int/>.
- 709 European Space Agency. (2020). Copernicus Sentinel-2 Mission: Calibration and Validation activities. *GS/CS  
710 Quarterly*, 14(1), Spring 2020 Issue. Retrieved from dlr.de
- 711 Fang, H., Baret, F., Plummer, S., Schaepman-Strub, G. (2019). An overview of global leaf area index (LAI):  
712 Methods, products, validation, and applications. *Reviews of Geophysics*, 57(4), 739–799,  
713 <https://doi.org/10.1029/2019RG000638>.

- 714 Fernandes, R., et al. (2021). LEAF Toolbox. Canada Centre for Remote Sensing. Retrieved from  
715 <https://github.com/ffernand387/LEAF-Toolbox/wiki> on March 15, 2023, Zenodo,  
716 <https://doi.org/10.5281/zenodo.4321298>.
- 717 Fernandes, R., Brown, L., Canisius, F., Dash, J., He, L., Hong, G., Huang, L., Le, N. Q., MacDougall, C., Meier,  
718 C., Darko, P. O., Shah, H., Spafford, L., Sun, L. (2023). Validation of simplified level 2 prototype processor  
719 Sentinel-2 fraction of canopy cover, fraction of absorbed photosynthetically active radiation, and leaf area  
720 index products over North American forests. *Remote Sensing of Environment*, 293, 113600,  
721 <https://doi.org/10.1016/j.rse.2023.113600>.
- 722 Fernandes, R., Djamai, N., Harvey, K., Hong, G., MacDougall, C., Shah, H., Sun, L. (2024a). Evidence of a  
723 bias-variance trade-off when correcting for bias in Sentinel-2 forest LAI retrievals using radiative transfer  
724 models. *Remote Sensing of Environment*, 305, 114060, <https://doi.org/10.1016/j.rse.2024.114060>.
- 725 Fernandes, R., Hong, G., Brown, L. A., Dash, J., Harvey, K., Kalimipalli, S., MacDougall, C., Meier, C., Morris,  
726 H., Shah, H., Sharma, A., Sun, L. (2024b). Not just a pretty picture: Mapping leaf area index at 10 m  
727 resolution using Sentinel-2. *Remote Sensing of Environment*, 311, 114269,  
728 <https://doi.org/10.1016/j.rse.2024.114269>.
- 729 Fernandes, R., Plummer, S., Nightingale, J., Baret, F., Camacho, F., Fang, H., Garrigues, S., Gobron, N., Lang,  
730 M., Lacaze, R., Leblanc, S., Meroni, M., Martinez, B., Nilson, T., Pinty, B., Pisek, J., Sonnentag, O., Verger,  
731 A., Welles, J., Weiss, M., Widlowski, J. L., Schaepman-Strub, G., Roman, M. (2014). Global leaf area index  
732 product validation good practices. In G. Schaepman-Strub, S. Plummer, J. Nightingale (Eds.), *Best Practice  
733 for Satellite-Derived Land Product Validation*. Land Product Validation Subgroup (Committee on Earth  
734 Observation Satellites Working Group on Calibration and Validation),  
735 <https://doi.org/10.5067/doc/ceoswgcv/lpv/lai.002>.
- 736 Ferchichi, A., Ben Abbes, A., Barra, V., Farah, I. R. (2022). Forecasting vegetation indices from spatio-  
737 temporal remotely sensed data using deep learning-based approaches: A systematic literature review.  
738 *Ecological Informatics*, 68, 101552, <https://doi.org/10.1016/j.ecoinf.2022.101552>.
- 739 Ganguly, S., Nemani, R. R., Zhang, G., Hashimoto, H., Milesi, C., Michaelis, A., Wang, W., Votava, P.,  
740 Samanta, A., Melton, F., Dungan, J. L., Vermote, E., Gao, F., Knyazikhin, Y., Myneni, R. (2012). Generating  
741 global leaf area index from Landsat: Algorithm formulation and demonstration. *Remote Sensing of  
742 Environment*, 122, 185–202, <https://doi.org/10.1016/j.rse.2011.11.017>.
- 743 Gao, L., Wang, X., Johnson, B. A., Tian, Q., Wang, Y., Verrelst, J., Mu, X., Gu, X. (2020). Remote sensing  
744 algorithms for estimation of fractional vegetation cover using pure vegetation index values: A review.  
745 *ISPRS Journal of Photogrammetry and Remote Sensing*, 159, 364–377,  
746 <https://doi.org/10.1016/j.isprsjprs.2019.11.018>.
- 747 Gascon, F., Bouzinac, C., Thepaut, O., Jung, M., Francesconi, B., Louis, J., Lonjou, V., Lafrance, B., Massera,  
748 S., Gaudel-Vacaresse, A., Languille, F., Alhammoud, B., Viallefond, F., Pflug, B., Bieniarz, J., Clerc, S., Pessiot,  
749 L., Trémas, T., Cadau, E., De Bonis, R., Isola, C., Martimort, P., Fernandez, V. (2017). Copernicus Sentinel-  
750 2A calibration and products validation status. *Remote Sensing*, 9(6), 584,  
751 <https://doi.org/10.3390/rs9060584>.

- 752 Giovos, R., Tassopoulos, D., Kalivas, D., Lougkos, N., Priovolou, A. (2021). Remote sensing vegetation  
753 indices in viticulture: A critical review. *Agriculture*, 11(5), 457,  
754 <https://doi.org/10.3390/agriculture11050457>.
- 755 Group on Earth Observation Global Agricultural Monitoring. (2023). *GEOGLAM initiative, stocktaking*  
756 *report 2023-India.* Retrieved from  
757 [https://earthobservations.org/documents/2023/G20\\_Stocktaking\\_2023\\_India.pdf](https://earthobservations.org/documents/2023/G20_Stocktaking_2023_India.pdf) (accessed June 2024).
- 758 Gonsamo, A., Chen, J. M. (2014). Improved LAI algorithm implementation to MODIS data by incorporating  
759 background, topography, and foliage clumping information. *IEEE Transactions on Geoscience and Remote*  
760 *Sensing*, 52(2), 1076-1088, <https://doi.org/10.1109/TGRS.2013.2247405>.
- 761 Group on Earth Observation Biodiversity Observation Network. (2023). *GEOBON strategic plan 2023-2026*  
762 (p. 20). Retrieved from <https://geobon.org/strategic-plan-new-version-v2>.
- 763 Ma, H., Liang, S. (2022). Development of the GLASS 250-m leaf area index product (version 6) from MODIS  
764 data using the bidirectional LSTM deep learning model. *Remote Sensing of Environment*, 273, 112985,  
765 <https://doi.org/10.1016/j.rse.2022.112985>.
- 766 Hermosilla, T., Wulder, M. A., White, J. C., Coops, N. C. (2019). Prevalence of multiple forest disturbances  
767 and impact on vegetation regrowth from interannual Landsat time series (1985–2015). *Remote Sensing of*  
768 *Environment*, 233, 111403, <https://doi.org/10.1016/j.rse.2019.111403>.
- 769 Hird, J. N., Kariyeva, J., McDermid, G. J. (2021). Satellite time series and Google Earth Engine democratize  
770 the process of forest-recovery monitoring over large areas. *Remote Sensing*, 13(23), 4745,  
771 <https://doi.org/10.3390/rs13234745>.
- 772 Kang, Y., Ozdogan, M., Gao, F., Anderson, M. C., White, W. A., Yang, Y., Erickson, T. A. (2021). A data-  
773 driven approach to estimate leaf area index for Landsat images over the contiguous US. *Remote Sensing*  
774 *of Environment*, 258, 112383, <https://doi.org/10.1016/j.rse.2021.112383>.
- 775 Knight, E. J., Kvaran, G. (2014). Landsat-8 Operational Land Imager design, characterization and  
776 performance. *Remote Sensing*, 6(11), 10286–10305, <https://doi.org/10.3390/rs611102860>.
- 777 Lacaze, R., Smets, B., Baret, F., Weiss, M., Ramon, D., Montersleet, B., Wandrebeck, L., Calvet, J. C.,  
778 Roujean, J. L., Camacho, F. (2015). Operational 333 m biophysical products of the Copernicus Global Land  
779 Service for agriculture monitoring. *The International Archives of the Photogrammetry, Remote Sensing*  
780 *and Spatial Information Sciences*, XL-7, 53–56, <https://doi.org/10.5194/isprsarchives-XL-7-W3-53-2015>.
- 781 Lang, A. R. G., Yueqin, X. (1986). Estimation of leaf area index from transmission of direct sunlight in  
782 discontinuous canopies. *Agricultural and Forest Meteorology*, 37(3), 229–243,  
783 [https://doi.org/10.1016/0168-1923\(86\)90033-X](https://doi.org/10.1016/0168-1923(86)90033-X).
- 784 Latifovic, R., Homer, C., Ressl, R., Pouliot, D. A., Hossian, S., Colditz, R., Olthof, I., Chandra, G., Victoria, A.  
785 (2012). North American land change monitoring system. In *Remote Sensing of Land Use and Land Cover: Principles and Applications* (pp. 303–324), <https://doi.org/10.1201/b11964-24>.

- 787 Levy, R., Miller, J. A., Barsi, J. A., Thome, K. J., Markham, B. L. (2024). Landsat 9 transfer to orbit of pre-  
788 launch absolute calibration of operational land imager (OLI). *Remote Sensing*, 16(8), 1360,  
789 <https://doi.org/10.3390/rs16081360>.
- 790 Müller-Wilm, U. (2018). *Sen2Cor configuration and user manual* (2nd ed.). CS, Toulouse, France.
- 791 Myneni, R. B., Ramakrishna, R., Nemani, R., Running, S. W. (1997). Estimation of global leaf area index and  
792 absorbed PAR using radiative transfer models. *IEEE Transactions on Geoscience and Remote Sensing*, 35(6),  
793 1380-1393, <https://doi.org/10.1109/36.649788>.
- 794 Niinemets, Ü., Tobias, M. (2019). Canopy leaf area index at its higher end: Dissection of structural controls  
795 from leaf to canopy scales in bryophytes. *New Phytologist*, 223(1), 118-133,  
796 <https://doi.org/10.1111/nph.15767>.
- 797 Pipia, L., Amin, E., Belda, S., Salinero-Delgado, M., Verrelst, J. (2021). Green LAI mapping and cloud gap-  
798 filling using Gaussian process regression in Google Earth Engine. *Remote Sensing*, 13(3), 403,  
799 <https://doi.org/10.3390/rs13030403>.
- 800 Putzenlechner, B., Castro, S., Kiese, R., Ludwig, R., Marzahn, P., Sharp, I., Sanchez-Azofifa, A. (2019).  
801 Validation of Sentinel-2 fAPAR products using ground observations across three forest ecosystems.  
802 *Remote Sensing of Environment*, 232, 111310, <https://doi.org/10.1016/j.rse.2019.111310>.
- 803 Putzenlechner, B., Marzahn, P., Sanchez-Azofifa, A. (2020). Accuracy assessment on the number of flux  
804 terms needed to estimate in situ fAPAR. *International Journal of Applied Earth Observation and  
805 Geoinformation*, 88, 102061, <https://doi.org/10.1016/j.jag.2020.102061>.
- 806 Qiu, S., Zhu, Z., He, B. (2019). Fmask 4.0: Improved cloud and cloud shadow detection in Landsats 4–8 and  
807 Sentinel-2 imagery. *Remote Sensing of Environment*, 231, 111205,  
808 <https://doi.org/10.1016/j.rse.2019.111205>.
- 809 Rochdi, N., Zhang, J., Staenz, K., Yang, X., David, R., Banting, J., King, C., Doherty, R. (2014). *Monitoring  
810 procedures for wellsite, in-situ oil sands and coal mine reclamation in Alberta (MOPRA)*. Oil Sands Research  
811 and Information Network, University of Lethbridge, <https://doi.org/10.7939/R3280505Q>.
- 812 Sanchez-Azofeifa, A., Sharp I., Green, P.D., and Nightingale, J. (2022). Calibration of Co-Located Identical  
813 PAR Sensors Using Wireless Sensor Networks and Characterization of the In Situ fPAR Variability in a  
814 Tropical Dry Forest. *Remote Sensing*, 14(12), 2752, <https://doi.org/10.3390/rs14122752>.
- 815 Storey, J., Choate, M., Lee, K. (2014). Landsat 8 Operational Land Imager on-orbit geometric calibration  
816 and performance. *Remote Sensing*, 6(11), 11127-11152, <https://doi.org/10.3390/rs6111127>.
- 817 Shabanov, N. V., Huang, D., Yang, W., Tan, B., Knyazikhin, Y., Myneni, R. B., Ahl, D. E., Gower, S. T., Huete,  
818 A. R., Aragao, L. E. O. C., Shimabukuro, Y. E. (2005). Analysis and optimization of the MODIS leaf area  
819 index algorithm retrievals over broadleaf forests. *IEEE Transactions on Geoscience and Remote Sensing*,  
820 43(8), 1855–1865, <https://doi.org/10.1109/TGRS.2005.852898>.
- 821 United States Geological Survey. (2019). *Landsat 8 data users handbook*. USGS. Retrieved from  
822 <https://www.usgs.gov/centers/eros/science/landsat-8-data-users-handbook>.

- 823 United States Geological Survey. (2022). *Landsat 9 data users handbook*. USGS. Retrieved from  
824 <https://www.usgs.gov/centers/eros/science/landsat-9-data-users-handbook>.
- 825 Verhoef, W. (1985). Earth observation modeling based on layer scattering matrices. *Remote Sensing of*  
826 *Environment*, 17(2), 165–178, [https://doi.org/10.1016/0034-4257\(85\)90072-0](https://doi.org/10.1016/0034-4257(85)90072-0)
- 827 Verhoef, W., Bach, H. (2007). Coupled soil–leaf-canopy and atmosphere radiative transfer modeling to  
828 simulate hyperspectral multi-angular surface reflectance and TOA radiance data. *Remote Sensing of*  
829 *Environment*, 109(2), 166–182, <https://doi.org/10.1016/j.rse.2006.12.021>.
- 830 Vermote, E., Roger, J. C., Franch, B., Skakun, S. (2018). LaSRC (Land Surface Reflectance Code): Overview,  
831 application and validation using MODIS, VIIRS, LANDSAT and Sentinel 2 data's. In *Proceedings of the IEEE*  
832 *International Geoscience and Remote Sensing Symposium* (Vol. 2018, pp. 8173-8176),  
833 <https://doi.org/10.1109/IGARSS.2018.8517622>.
- 834 Wan, L., Ryu, Y., Dechant, B., Hwang, Y., Feng, H., Kang, Y., Jeong, S., Lee, J., Choi, C., Bae, J. (2024).  
835 Correcting confounding canopy structure, biochemistry and soil background effects improves leaf area  
836 index estimates across diverse ecosystems from Sentinel-2 imagery. *Remote Sensing of Environment*, 309,  
837 114224, <https://doi.org/10.1016/j.rse.2024.114224>.
- 838 Weiss, M., Baret, F. (2016). *S2ToolBox level 2 products: Version 1.1*. Available online: ATBD\_S2ToolBox  
839 (esa.int).
- 840 Weiss, M., Baret, F. (2020). *S2ToolBox level 2 products: Version 2.0*. Available online: ATBD\_S2ToolBox  
841 (esa.int).
- 842 WGClimate. (2017). *Space agency response to GCOS implementation plan*. The Joint CEOS/CGMS Working  
843 Group on Climate (WGClimate). ESA-ECO-EOPS-WGCL-RP-17-0061, Version 1.0.
- 844 Widlowski, J. L., Taberner, M., Pinty, B., Bruniquel-Pinel, V., Disney, M., et al. (2007). Third Radiation  
845 Transfer Model Intercomparison (RAMI) exercise: Documenting progress in canopy reflectance models.  
846 *Journal of Geophysical Research*, 112(D9), D09111, <https://doi.org/10.1029/2006JD007821>.
- 847 World Meteorological Organization (WMO), United Nations Environment Programme (UNEP),  
848 International Science Council (ISC), Intergovernmental Oceanographic Commission of the United Nations  
849 Educational, Scientific and Cultural Organization (IOC-UNESCO). (2022). *The 2022 GCOS ECV requirements*  
850 (GCOS-245). Retrieved from <https://www.wmo.int>.
- 851 Yan, K., Park, T., Chen, C., Xu, B., Song, W., Yang, B., Zeng, Y., Liu, Z., Yan, G., Knyazikhin, Y., Myneni, R. B.  
852 (2018). Generating global products of LAI and FPAR from SNPP-VIIRS data: Theoretical background and  
853 implementation. *IEEE Transactions on Geoscience and Remote Sensing*, 56(4), 2119-2137,  
854 <https://doi.org/10.1109/TGRS.2017.2775247>.
- 855 Yan, K., Park, T., Yan, G., Chen, C., Yang, B., Liu, Z., Nemani, R., Knyazikhin, Y., Myneni, R. (2016). Evaluation  
856 of MODIS LAI/FPAR product collection 6. Part 1: Consistency and improvements. *Remote Sensing*, 8(5),  
857 359, <https://doi.org/10.3390/rs8050359>.

- 858 Zotz, G., Kahler, H. (2007). A moss “canopy”—Small-scale differences in microclimate and physiological  
859 traits in *Tortula ruralis*. *Flora-Morphology, Distribution, Functional Ecology of Plants*, 202(8), 661-666,  
860 <https://doi.org/10.1016/j.flora.2007.05.004>.
- 861 Zupanc, A. (2017). Improving cloud detection with machine learning. *Sentinel Hub Blog*. Medium.  
862 Retrieved from <https://medium.com/sentinel-hub/improving-cloud-detection-with-machine-learning-2b458d340be1>.

864

# Appendix A

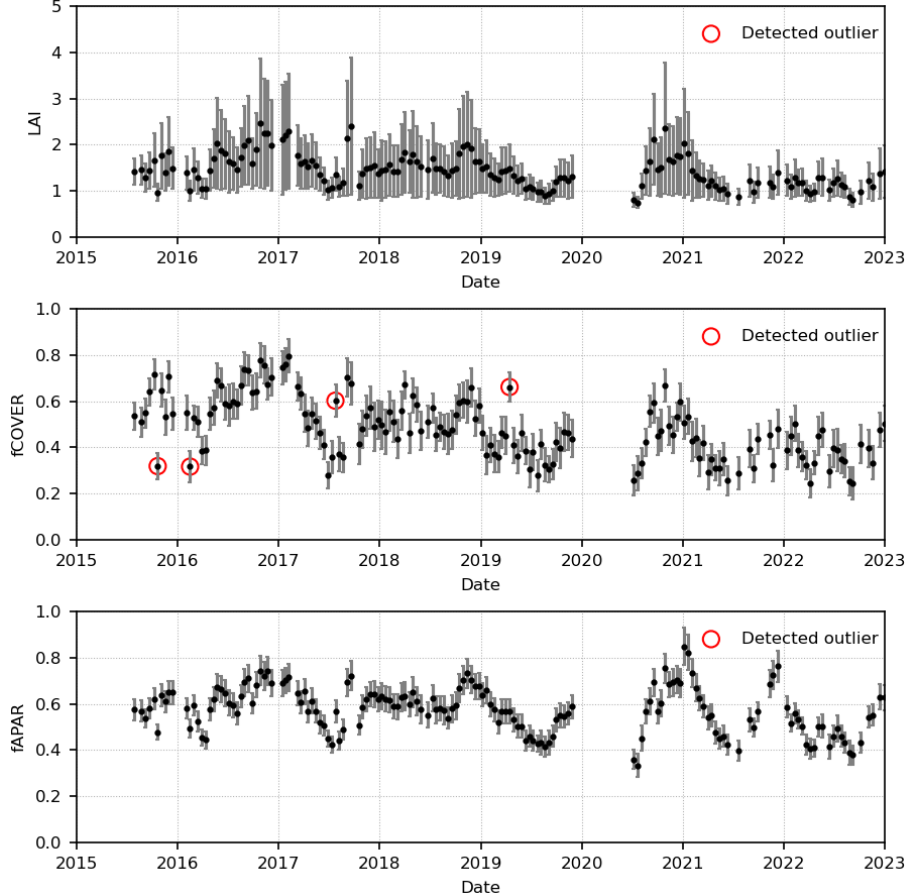
865 *Table A1. Number of ESUs, sampling period, number of acquired samples, and NLCD classes for CCRS and*  
 866 *NEON sites.*

Site	Network	Start Date	End Date	#ESUs	NLCD (#samples)
Peace River	CCRS	2019-08-12	2019-08-12	3	DF (3)
YellowKnife	CCRS	2019-08-11	2019-08-12	3	EF (3)
Mer Bleue	CCRS	2019-09-18	2019-09-18	3	EF (2), DF (1)
Hay River	CCRS	2019-09-05	2019-09-07	28	EF (27), MF (1)
Geraldton	CCRS	2020-07-21	2020-07-21	3	EF (2), DF (1)
Nova Scotia	CCRS	2021-08-26	2021-08-27	3	EF (2), DF (1)
Turkey Point	CCRS	2019-06-27	2019-06-27	3	EF (2), DF (1)
Vancouver Island	CCRS	2019-08-09	2019-08-10	3	EF (3)
Mt. Polley	CCRS	2019-08-14	2019-08-15	3	MF (2), EF (1)
Labrador	CCRS	2019-07-24	2019-07-31	12	MF (6), EF (6)
STER	NEON	2014-04-01	2022-09-08	19	CC (357)
KONA	NEON	2017-06-22	2022-10-27	24	CC (221)
TREE	NEON	2015-07-08	2022-06-21	23	DF (145), MF (79), WW (11), EF (3)
UKFS	NEON	2016-04-06	2022-10-25	24	DF (268), EF (55), GH (3)
BART	NEON	2016-04-14	2022-11-17	27	DF (234), MF (128), EF (11)
SERC	NEON	2017-06-16	2022-09-12	25	DF (356), CC (6)
SCBI	NEON	2015-04-29	2022-09-26	27	DF (402), PH (8)
STEI	NEON	2014-05-08	2022-10-18	23	DF (259), MF (3), WW (3)
BLAN	NEON	2015-09-12	2022-06-21	22	DF (126), SS (118), CC (115), PH (10)
CLBJ	NEON	2016-03-23	2022-11-01	25	DF (328), GH (20)
ORNL	NEON	2016-03-09	2022-11-27	31	DF (416), EF (12), PH (9)
LENO	NEON	2014-06-06	2022-09-26	23	DF (193), WW (114)
GRSM	NEON	2017-08-14	2022-10-04	23	DF (319), EF (4)
MLBS	NEON	2016-06-08	2022-12-03	23	DF (214)
BONA	NEON	2014-06-04	2022-10-25	25	DF (93), EF (77), SS (6), MF (3), WW (2)
DELA	NEON	2015-04-19	2022-10-03	26	DF (294), WW (34), EF (4)
HEAL	NEON	2017-07-17	2022-08-22	23	DS (160), SS (15), EF (1)
BARR	NEON	2018-04-26	2022-08-23	23	EHW (64), SH (15)
TEAK	NEON	2013-04-17	2022-08-10	20	EF (91), SS (1)
JERC	NEON	2015-07-28	2022-12-29	26	EF (364), DF (7), MF (4), CC (3)
SOAP	NEON	2018-07-30	2021-09-22	23	EF (150), SS (2)
ABBY	NEON	2016-11-01	2022-11-24	18	EF (139), GH (68), SS (3), MF (1)
YELL	NEON	2018-06-12	2022-11-01	17	EF (72), SS (10), GH (1)
GUAN	NEON	2019-06-13	2022-09-27	24	EF (518)
SJER	NEON	2014-05-16	2022-10-12	23	EF (207), DF (101), GH (30), SS (4)
RMNP	NEON	2016-07-06	2022-09-12	25	EF (82), DF (58), MF (57)
PUUM	NEON	2013-06-11	2022-08-04	23	EF (320)
OSBS	NEON	2017-08-04	2022-10-25	34	EF (435), WW (22), DF (7), MF (6), EHW (4)
WREF	NEON	2018-04-10	2022-11-01	27	EF (176)
DEJU	NEON	2016-08-25	2022-07-05	23	EF (160), SS (8), WW (2)
TALL	NEON	2016-03-16	2022-10-27	23	EF (390), DF (12), MF (9)
KONZ	NEON	2016-05-10	2022-10-17	24	GH (348), DF (4)
NOGP	NEON	2015-07-14	2022-09-19	23	GH (274)

NIWO	NEON	2017-06-19	2022-10-19	24	GH (188), EF (13)
DCFS	NEON	2014-03-26	2022-10-26	23	GH (247)
C PER	NEON	2014-05-08	2022-10-19	23	GH (451)
WOOD	NEON	2014-05-01	2022-10-24	27	GH (361), EHW (11)
HARV	NEON	2014-05-20	2022-07-12	21	MF (244), EF (126), DF (6), WW (2)
UNDE	NEON	2016-04-15	2022-12-29	27	MF (105), WW (100), DF (81)
LAJA	NEON	2013-02-11	2022-09-21	4	PH (455), EF (1)
DSNY	NEON	2017-07-10	2022-08-15	24	PH (452), WW (36)
TOOL	NEON	2021-07-15	2021-07-22	22	SH (111), DS (20), SS (2)
SRER	NEON	2016-04-27	2022-10-24	23	SS (339)
JORN	NEON	2015-06-10	2022-11-01	23	SS (335)
OAES	NEON	2016-03-21	2022-11-15	20	SS (213), GH (110)
ONAQ	NEON	2014-05-22	2022-09-13	23	SS (337), EF (13)
MOAB	NEON	2015-05-13	2022-11-01	23	SS (311), EF (3)

867

868 **Appendix B**



869

870 *Figure B1. Example of outliers detected on RMs time series acquired on NEON ESU GUAN\_054*

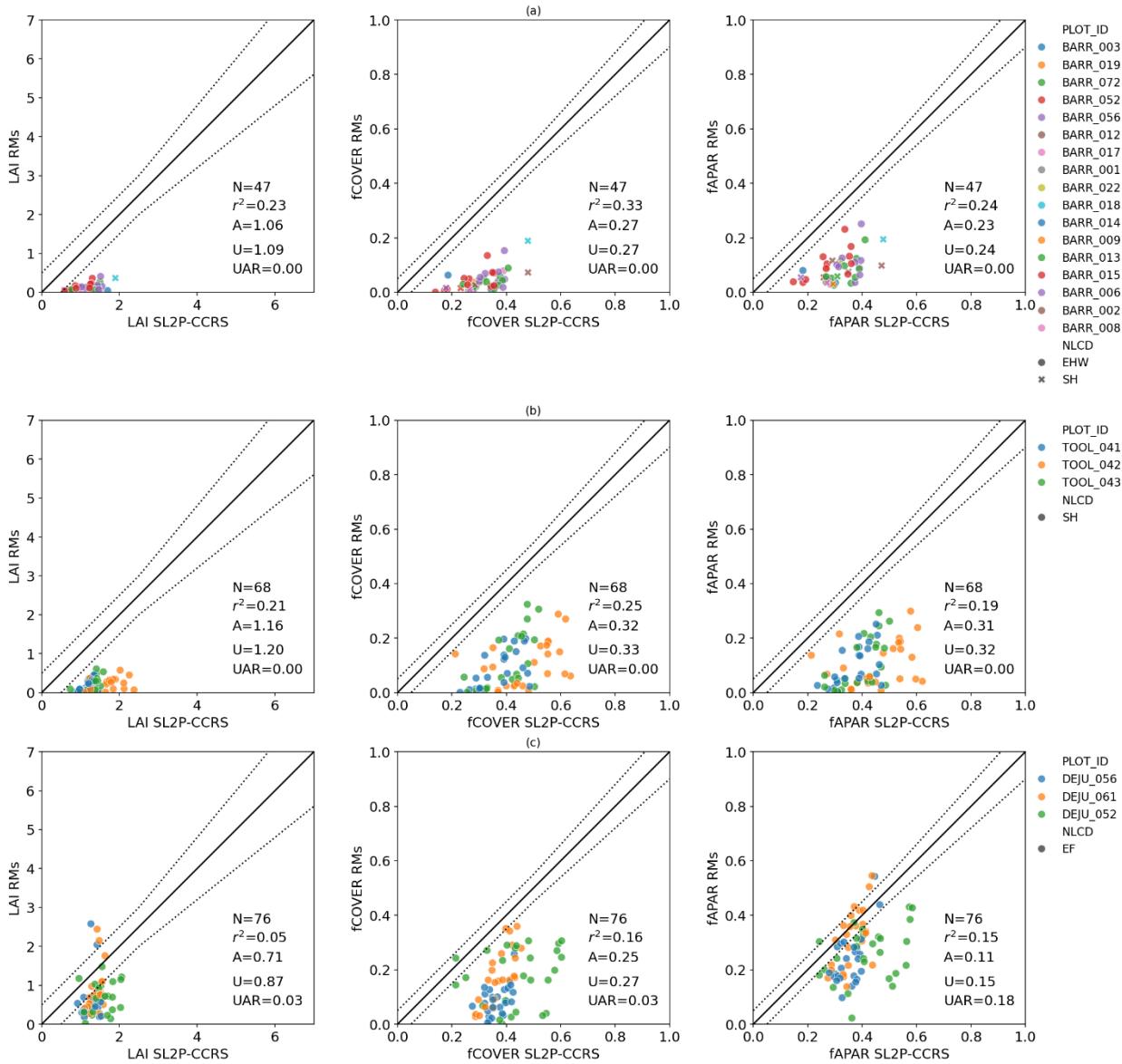
871 *Table B1. Number of samples (N) and number and percentage of outliers detected for each variable and*  
872 *NLCD class for NEON sites.*

NLCD	LAI			fCOVER			fAPAR		
	N	#Outliers	%	N	#Outliers	%	N	#Outliers	%
EF	3427	3	0.09	3427	30	0.88	3427	16	0.47
GH	2101	1	0.05	2101	4	0.19	2101	3	0.14
SS	1704	0	0	1704	1	0.06	1704	1	0.06
MF	639	1	0.16	639	1	0.16	639	1	0.16
SH	126	0	0	126	0	0	126	0	0
EHW	79	0	0	79	0	0	79	0	0
DF	3923	19	0.48	3923	28	0.71	3923	31	0.79
PH	934	16	1.71	934	55	5.89	934	48	5.14
CC	702	2	0.28	702	16	2.28	702	16	2.28
WW	326	2	0.61	326	2	0.61	326	2	0.61
Total	13961	44	0.31	13961	137	0.97	13961	118	0.83

873

874

## Appendix C



875

876 *Figure C1.* Scatter plots of SL2P-CCRS estimates of LAI, fCOVER and fAPAR obtained from S2 data versus  
 877 matching RMSEs for (a) BARR, (b) TOOL and (c) DEJU sedge sites, together with population validation  
 878 metrics. Dashed lines bound target user requirement around solid 1:1 line.

879

880 *Table C1.* Woody-to-total area ratios and their uncertainties, in parentheses, applied to RMSEs. Site  
 881 corresponds to NEON site ID (Appendix A) or all sites with corresponding SL2P-CCRS land cover  
 882 classification and overstory canopy height <19m.

NLCD (site)	Overstory	Understory	Source
DF (<19m)	0.24 (0.11)	0.05	Brown et al., 2021

MF (<19m)	0.18 (0.11)	0.05	Brown et al., 2021
OTHER (<19m)	0.10 (0.11)	0.05	Brown et al., 2021
EF (others)	0.16 (0.10)	0.05	Brown et al., 2021
EF (ABBY)	0.70 (0.19)	0.05	this study
EF (WREF)	0.75 (0.19)	0.05	this study
EF (PUUM)	0.65 (0.19)	0.05	this study
EF (TEAK)	0.60 (0.19)	0.05	this study

883

884 **Appendix D**

885 *Table D1. R<sup>2</sup>, A, P and U statistics for SL2P-CCRS estimates of LAI, fCOVER and fAPAR from LS data versus*  
 886 *matching RMs, as well as the samples size (N) and the variation range (min max) of RMs.*

NLCD	LAI						fCOVER						fAPAR					
	N	R <sup>2</sup>	A	U	min	max	N	R <sup>2</sup>	A	U	min	max	N	R <sup>2</sup>	A	U	min	max
EHW	35	0.57	0.12	0.31	0.58	2.07	35	0.65	0.04	0.09	0.12	0.61	35	0.83	0.03	0.07	0.14	0.59
SH	69	0.40	0.01	0.22	0.71	1.88	69	0.56	0.02	0.07	0.24	0.61	69	0.51	0.02	0.07	0.22	0.59
CC	234	0.79	0.30	0.50	0.08	3.95	234	0.82	0.11	0.15	0.00	0.84	234	0.86	0.07	0.11	0.03	0.83
PH	383	0.68	0.39	0.59	0.57	3.81	383	0.69	0.11	0.17	0.04	0.85	383	0.68	0.06	0.13	0.03	0.83
SS	614	0.92	0.26	0.67	0.19	5.88	614	0.90	0.06	0.10	0.00	0.96	614	0.89	0.05	0.10	0.00	0.93
GH	1136	0.72	0.38	0.57	0.10	5.64	1136	0.76	0.11	0.15	0.00	0.93	1136	0.78	0.08	0.13	0.01	0.91
WW	138	0.72	-1.50	1.87	0.58	5.40	138	0.61	-0.09	0.16	0.19	0.89	138	0.46	-0.17	0.22	0.18	0.86
MF	319	0.75	-1.30	1.51	0.52	4.72	319	0.85	-0.05	0.09	0.16	0.89	319	0.73	-0.11	0.15	0.18	0.86
DF	1816	0.74	-1.27	1.68	0.03	5.53	1816	0.76	-0.04	0.12	0.03	0.94	1816	0.73	-0.09	0.15	0.03	0.91
EF	1825	0.67	-0.38	0.82	0.02	4.28	1825	0.71	-0.01	0.12	0.01	0.87	1825	0.67	-0.08	0.14	0.02	0.85
All	6569	0.82	-0.43	1.13	0.02	5.88	6569	0.83	0.02	0.13	0.00	0.96	6569	0.80	-0.03	0.14	0.00	0.93

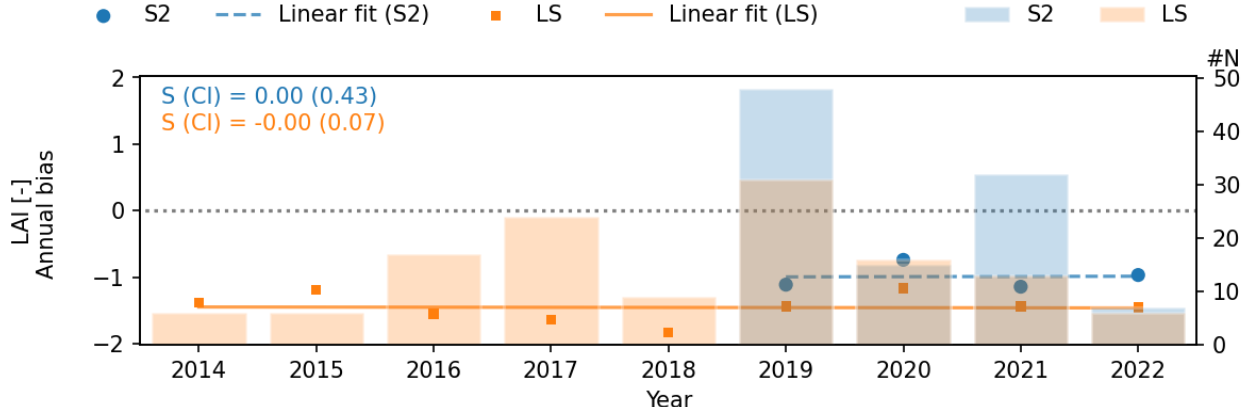
887

888 *Table D2. R<sup>2</sup>, A, P and U statistics for SL2P-CCRS estimates of LAI, fCOVER and fAPAR from S2 data versus*  
 889 *matching RMs, as well as the samples size (N) and the variation range (min max) of RMs.*

NLCD	LAI						fCOVER						fAPAR					
	N	R <sup>2</sup>	A	U	min	max	N	R <sup>2</sup>	A	U	min	max	N	R <sup>2</sup>	A	U	min	max
EHW	40	0.49	0.26	0.35	0.12	1.70	40	0.54	0.02	0.06	0.03	0.41	40	0.51	0.02	0.06	0.04	0.41
SH	79	0.24	0.11	0.32	0.59	2.37	79	0.58	0.01	0.07	0.21	0.64	79	0.54	0.01	0.07	0.21	0.62
CC	163	0.77	0.36	0.57	0.01	4.03	163	0.79	0.10	0.15	0.00	0.90	163	0.82	0.07	0.12	0.01	0.88
PH	319	0.63	0.45	0.66	0.15	4.85	319	0.64	0.11	0.17	0.06	0.88	319	0.69	0.06	0.13	0.07	0.86
SS	420	0.86	0.17	0.66	0.00	5.89	420	0.88	0.07	0.11	0.00	0.92	420	0.88	0.05	0.10	0.00	0.90
GH	747	0.75	0.27	0.60	0.00	4.95	747	0.81	0.10	0.14	0.00	0.90	747	0.83	0.05	0.11	0.00	0.85
WW	83	0.63	-1.73	1.99	0.63	5.38	83	0.52	-0.11	0.17	0.20	0.91	83	0.46	-0.17	0.21	0.18	0.89
MF	195	0.84	-1.01	1.21	0.29	5.22	195	0.86	-0.01	0.09	0.03	0.92	195	0.80	-0.09	0.13	0.01	0.89
DF	1330	0.73	-0.87	1.36	0.10	6.87	1330	0.74	-0.02	0.13	0.01	0.99	1330	0.73	-0.08	0.15	0.04	0.95
EF	1556	0.66	-0.39	0.81	0.16	5.00	1556	0.69	0.01	0.12	0.01	0.87	1556	0.67	-0.06	0.13	0.06	0.84
All	4932	0.80	-0.33	0.98	0.00	6.87	4932	0.81	0.03	0.13	0.00	0.99	4932	0.79	-0.03	0.13	0.00	0.95

890

891 **Appendix E**



892  
893 *Figure E1. NEON UNDE site SL2P-CCRS LAI number of annual matchups (N), annual bias time series,*  
894 *ordinary linear regression fits for S2 (blue bars, dots, and dashed line, respectively) and LS (orange bars,*  
895 *dots, and solid line, respectively). The expected value and 95% confidence interval of S, corresponding to*  
896 *the fitted line slope, are indicated for S2 (blue text) and LS (orange text).*

897

898 *Table E1. Class specific statistics between SL2P-CCRS estimates from LS data versus the corresponding*  
899 *estimates from S2 data (reference), conjointly with the samples size and the variation range of estimates*  
900 *from S2.*

NLCD	LAI						fCOVER						fAPAR					
	N	R2	A	U	min	max	N	R2	A	U	min	max	N	R2	A	U	min	max
EHW	784	0.76	0.03	0.3	0.01	3.9	785	0.74	0.02	0.08	0	0.8	786	0.71	0.02	0.08	0.01	0.78
SH	464	0.8	0.01	0.17	0.17	2.65	464	0.85	0.04	0.06	0.1	0.68	464	0.83	0.04	0.06	0.12	0.66
CC	1169	0.91	0.07	0.38	0	6.92	1078	0.94	0.02	0.07	0	0.98	1312	0.95	0.03	0.07	0	0.95
PH	873	0.89	-0.01	0.37	0.02	6.64	874	0.89	0.01	0.07	0	0.95	876	0.89	0.01	0.07	0.01	0.93
SS	8240	0.92	0.15	0.27	0	7.4	7601	0.95	-0.01	0.04	0	0.98	7649	0.93	0	0.05	0	0.97
GH	8117	0.9	0.14	0.29	0	5.6	8147	0.93	0.02	0.06	0	0.94	8907	0.93	0.03	0.06	0	0.91
WW	3245	0.82	-0.22	0.61	0.02	6.39	3246	0.88	-0.02	0.07	0.03	0.96	3246	0.88	-0.02	0.08	0.02	0.93
MF	2053	0.81	-0.13	0.56	0.17	6.09	2053	0.86	-0.03	0.08	0.1	0.96	2053	0.84	-0.04	0.09	0.1	0.93
DF	10043	0.87	-0.34	0.8	0.02	7.59	10050	0.92	-0.03	0.08	0.01	1.01	10051	0.92	-0.03	0.08	0	0.98
EF	11805	0.83	-0.1	0.38	0	5.37	11801	0.86	-0.04	0.08	0	0.93	11807	0.85	-0.04	0.08	0.01	0.9
All	46793	0.89	-0.07	0.5	0.02	6.39	46099	0.93	-0.01	0.07	0.03	0.96	47151	0.92	-0.01	0.07	0.02	0.93

901

902 **Appendix F**

903 *Table F1. The correlation coefficient R (and the corresponding coefficient interval) between S for SL2P-*  
 904 *CCRS estimates of LAI, fCOVER and fAPAR from LS data and the mean annual bias (mean RM<sub>s</sub>)*

Variable	S vs. Annual bias mean			S vs. RM <sub>s</sub> mean		
	R	CI (low)	CI (high)	R	CI (low)	CI (high)
LAI	0.43	0.15	0.64	-0.41	-0.63	-0.13
fCOVER	0.10	-0.20	0.38	-0.02	-0.30	0.28
fAPAR	0.06	-0.24	0.34	-0.03	-0.32	0.26

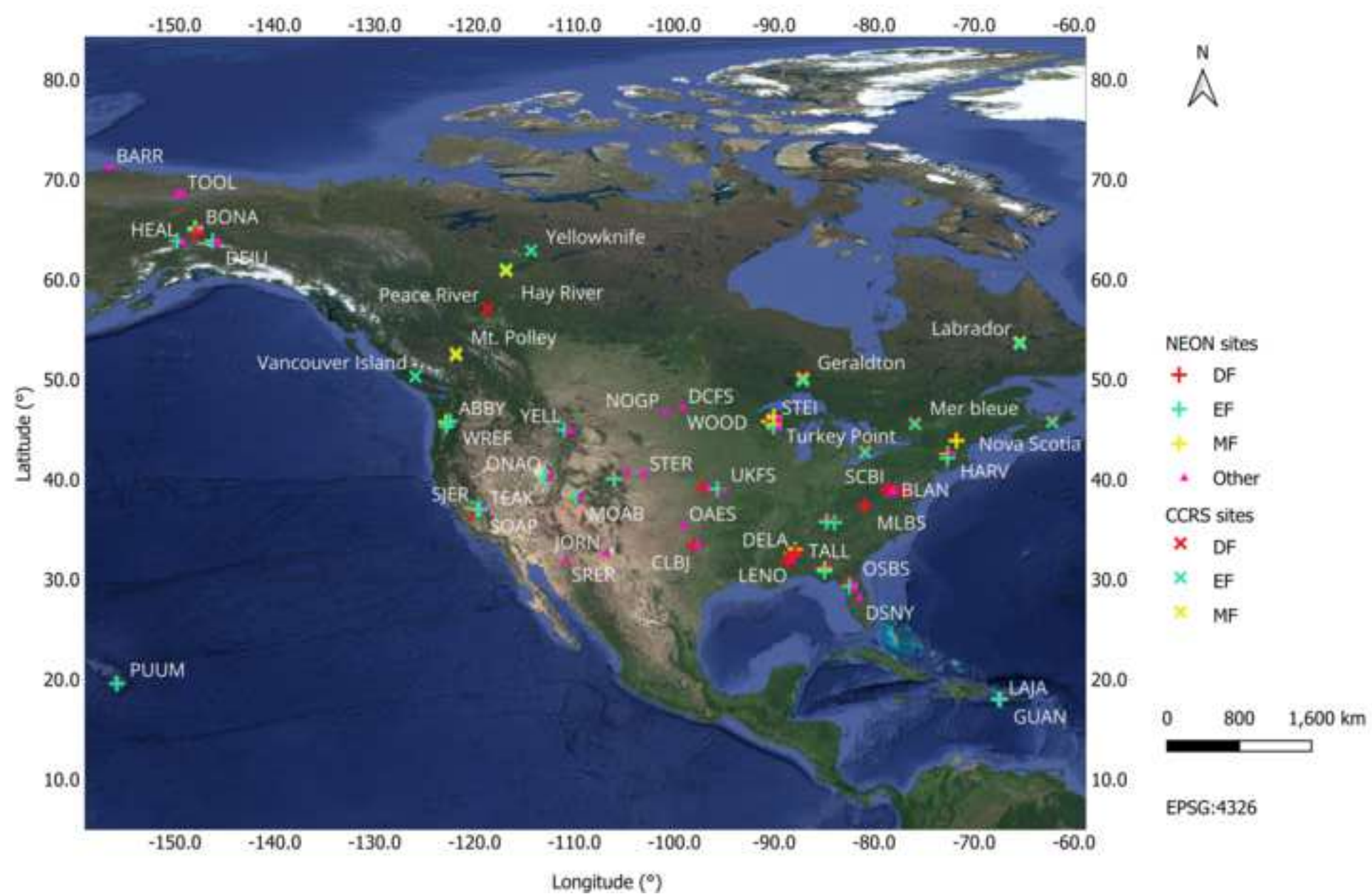
905

906 *Table F2. The correlation coefficient R (and the corresponding coefficient interval) between S for SL2P-*  
 907 *CCRS estimates of LAI, fCOVER and fAPAR from S2 data and the mean annual (mean RM<sub>s</sub>)*

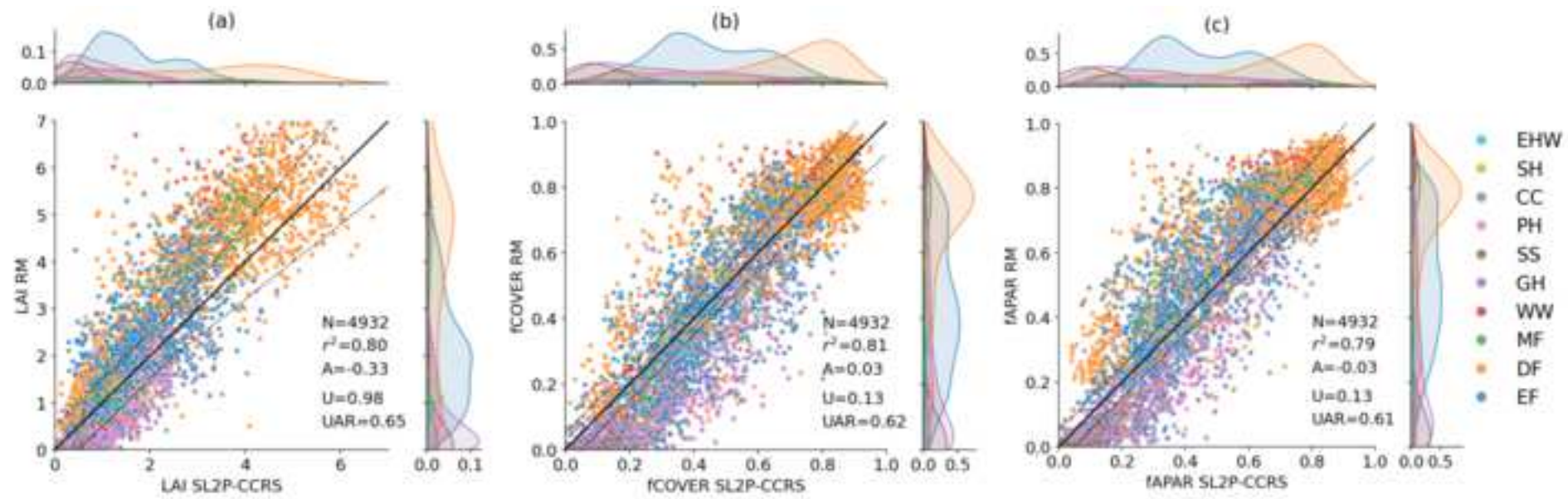
Variable	S vs. Annual bias mean			S vs. RM <sub>s</sub> mean		
	R	CI (low)	CI (high)	R	CI (low)	CI (high)
LAI	-0.13	-0.47	0.24	0.22	-0.15	0.54
fCOVER	-0.06	-0.42	0.31	0.00	-0.37	0.36
fAPAR	0.18	-0.18	0.50	-0.16	-0.48	0.20

908

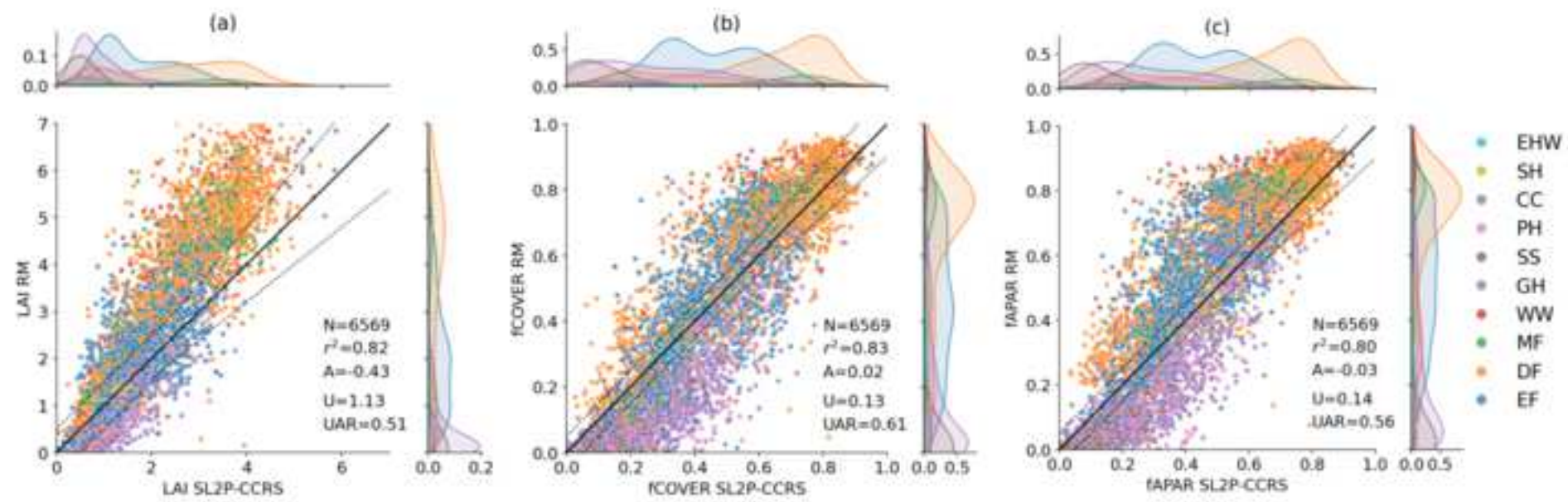
Figure\_1

[Click here to download Figure\\_1.png](#)

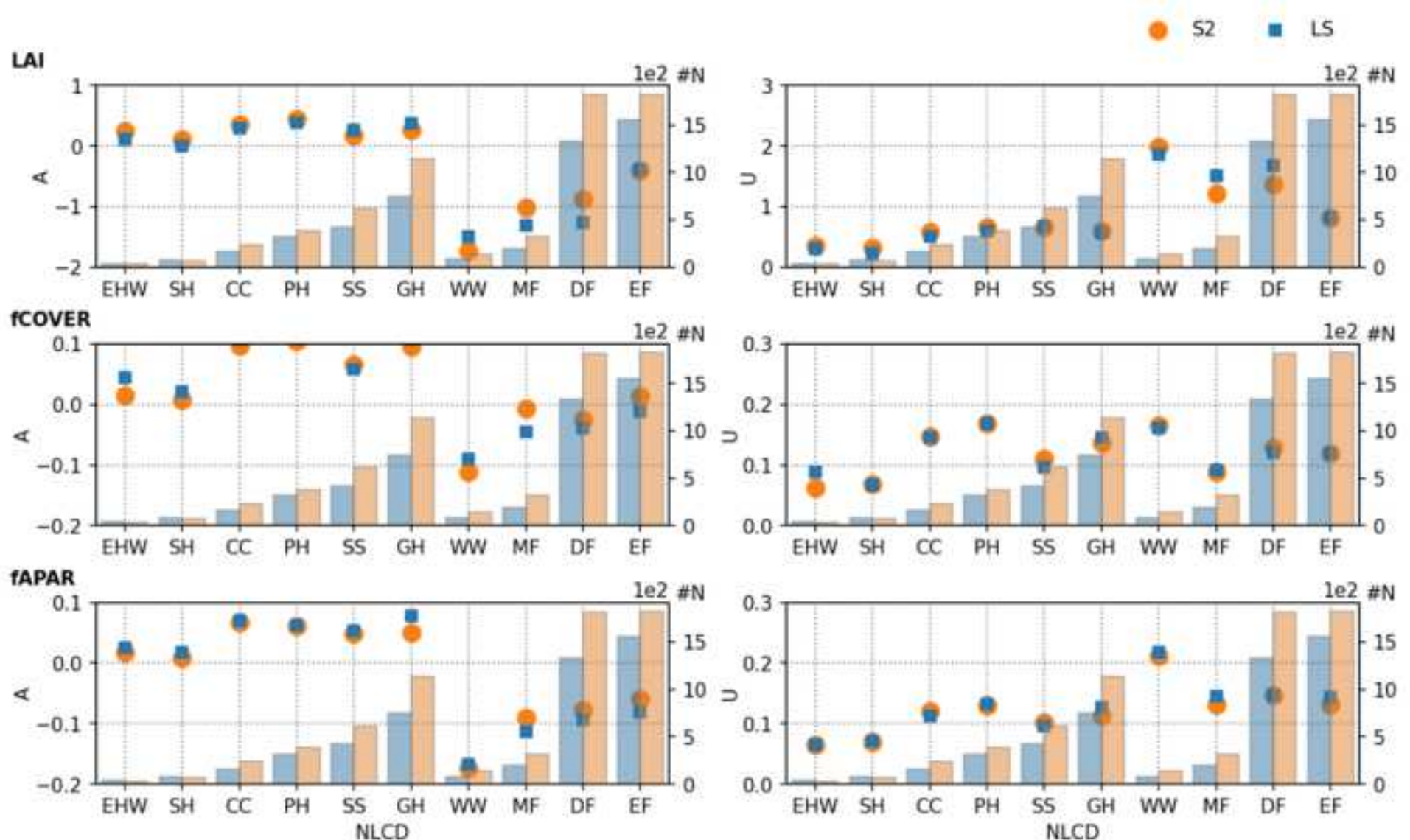
Figure\_2

[Click here to download Figure Figure\\_2.png](#)

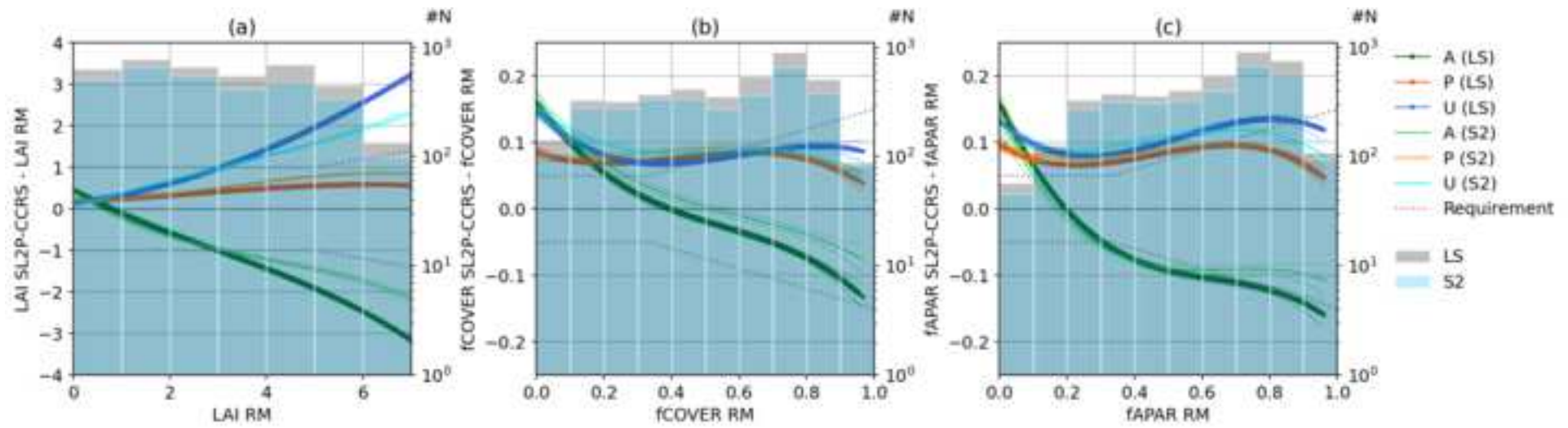
Figure\_3

[Click here to download Figure Figure\\_3.png](#)

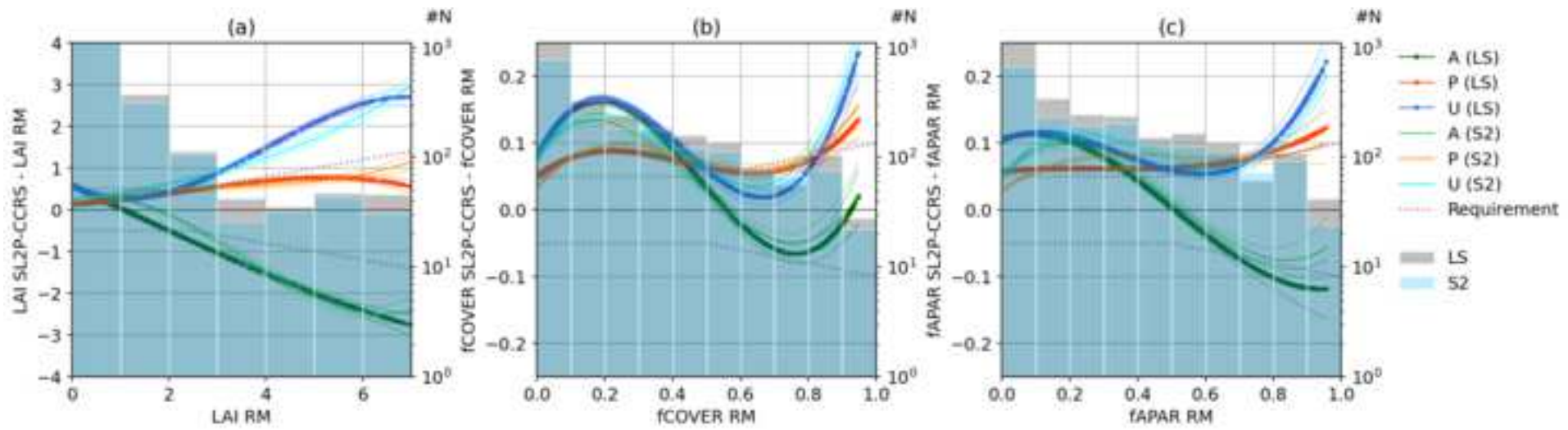
Figure\_4

[Click here to download Figure Figure\\_4.png](#)


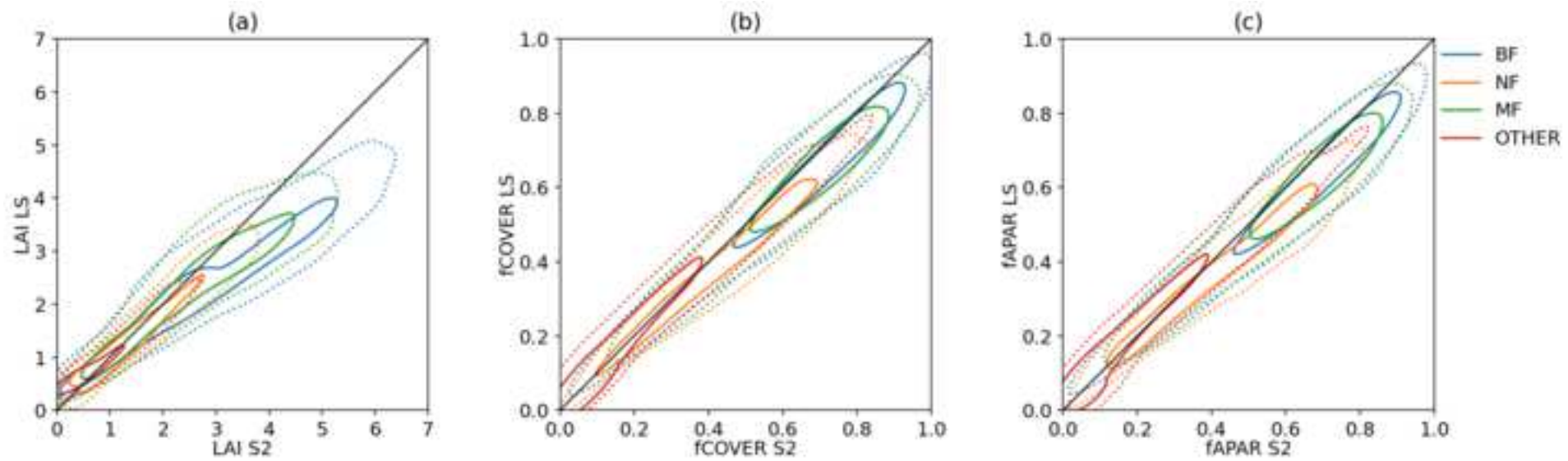
Figure\_5

[Click here to download Figure Figure\\_5.png](#)

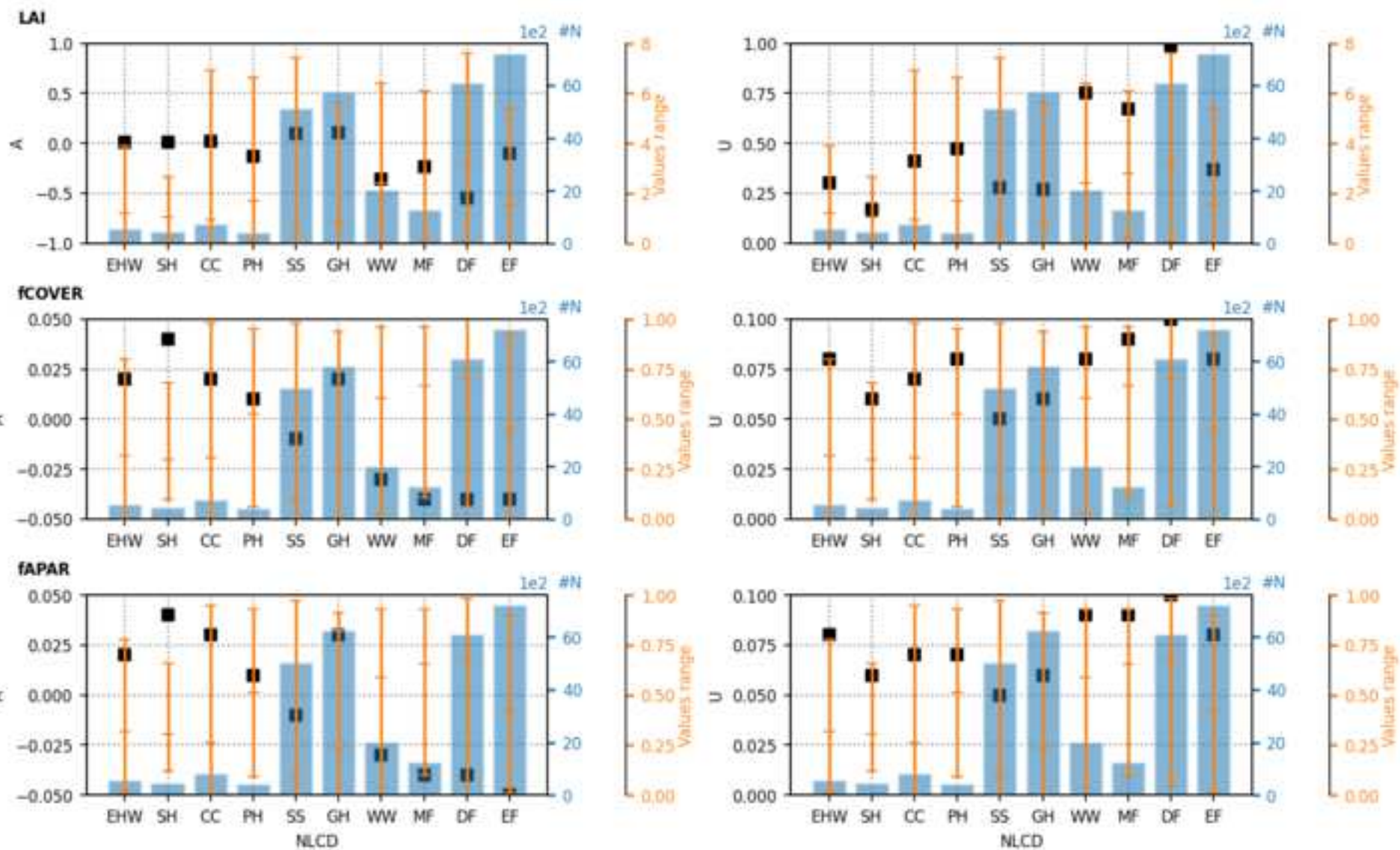
Figure\_6

[Click here to download Figure Figure\\_6.png](#)

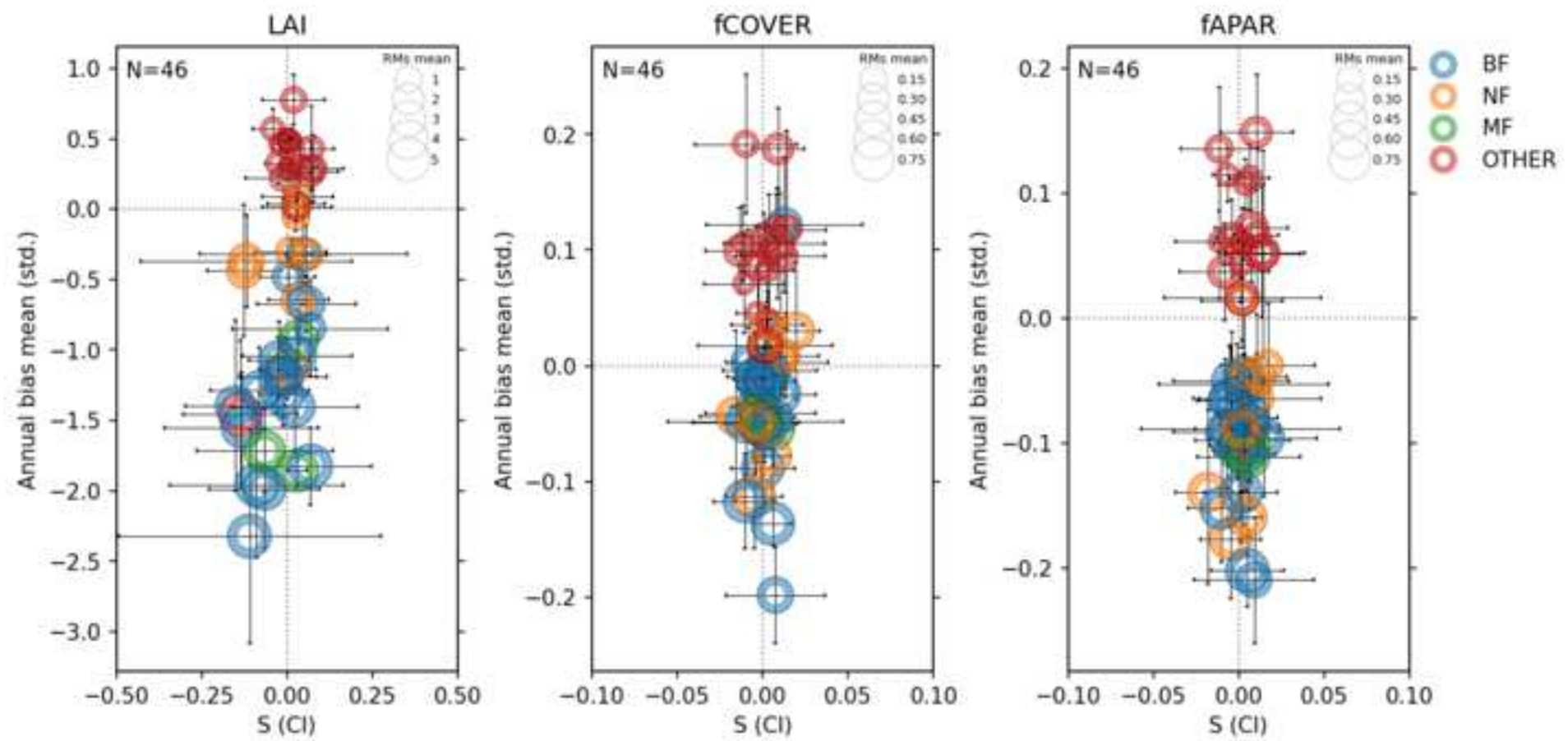
Figure\_7

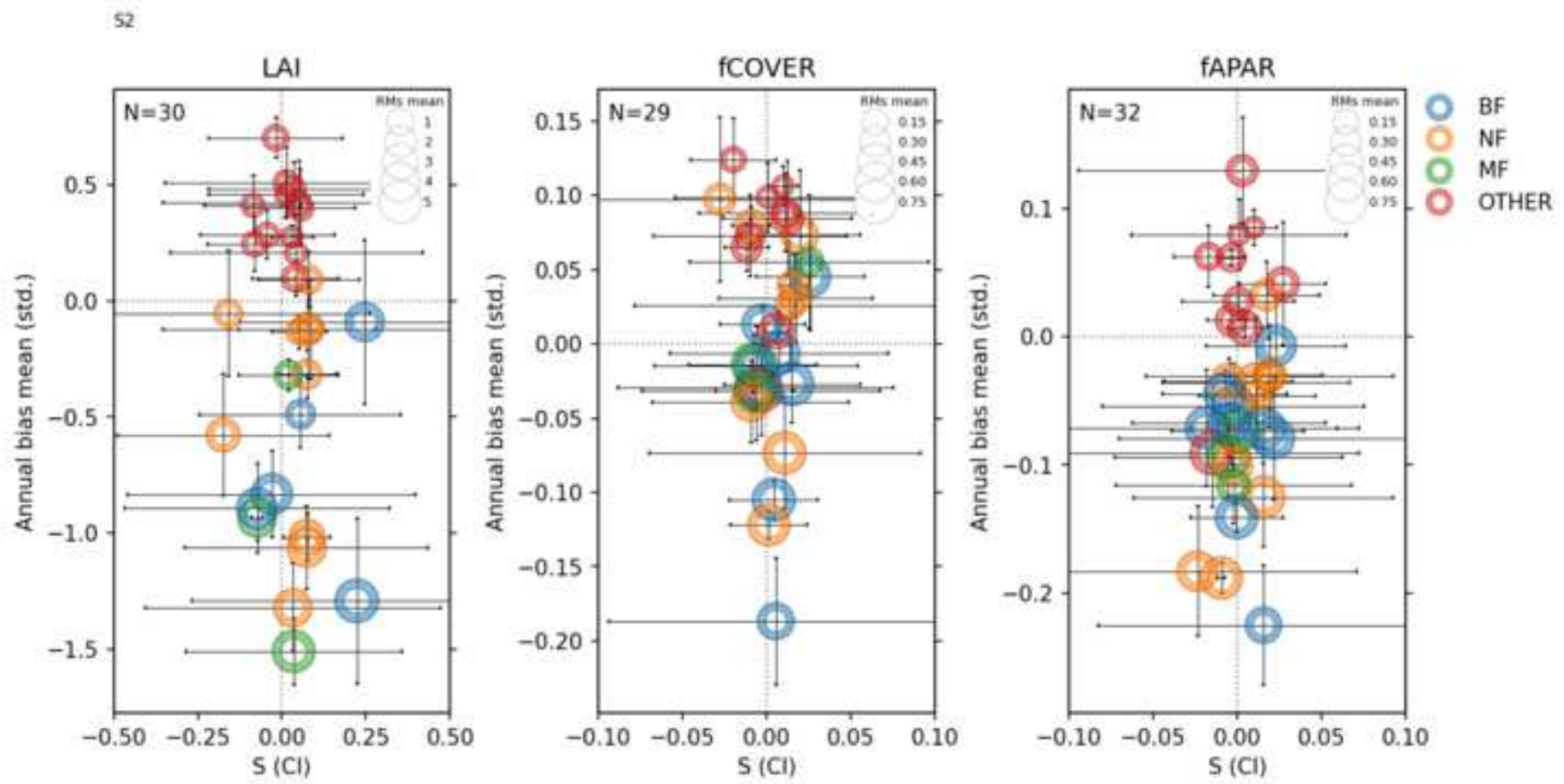
[Click here to download Figure Figure\\_7.png](#)

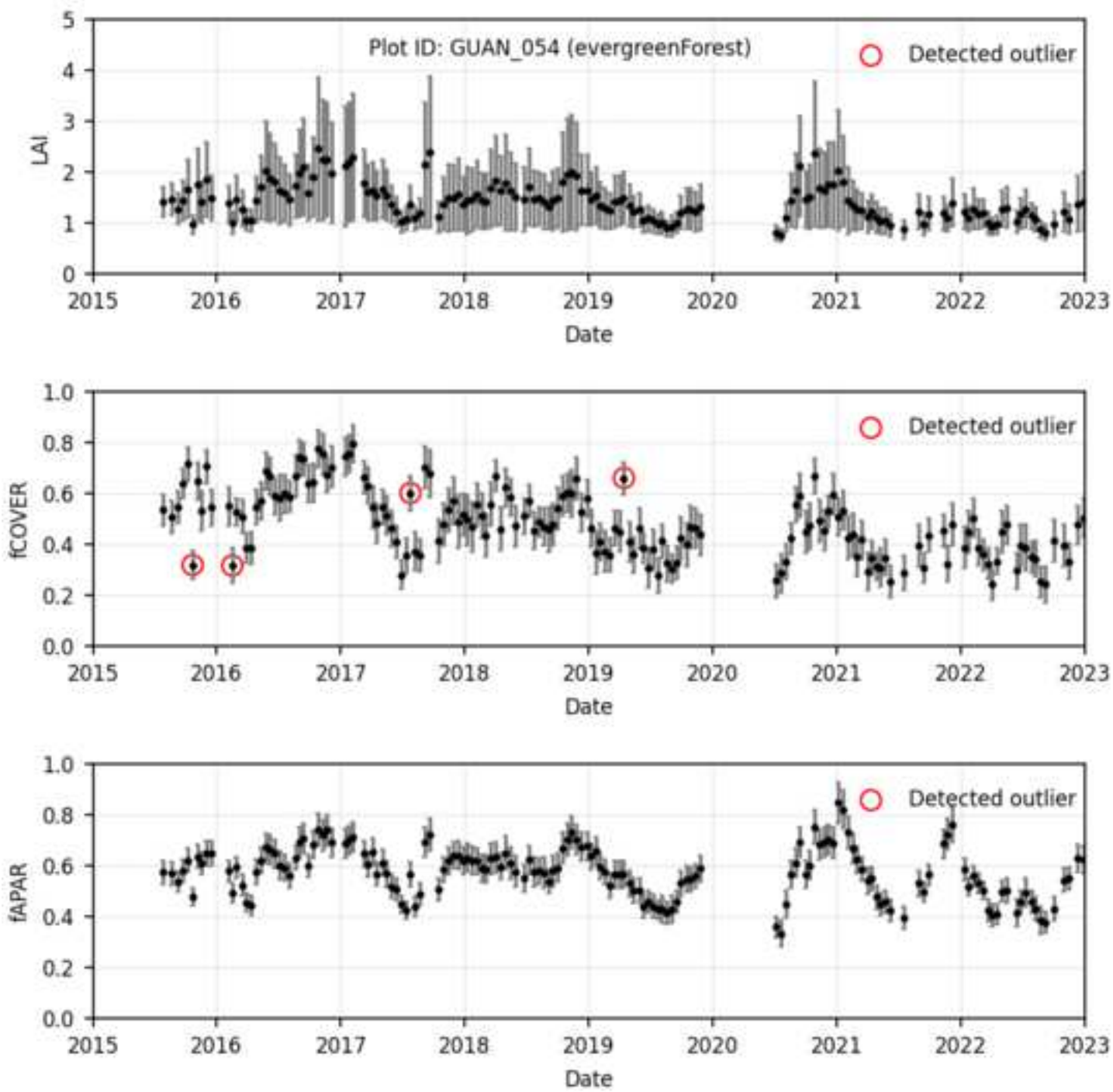
Figure\_8

[Click here to download Figure Figure\\_8.png](#)


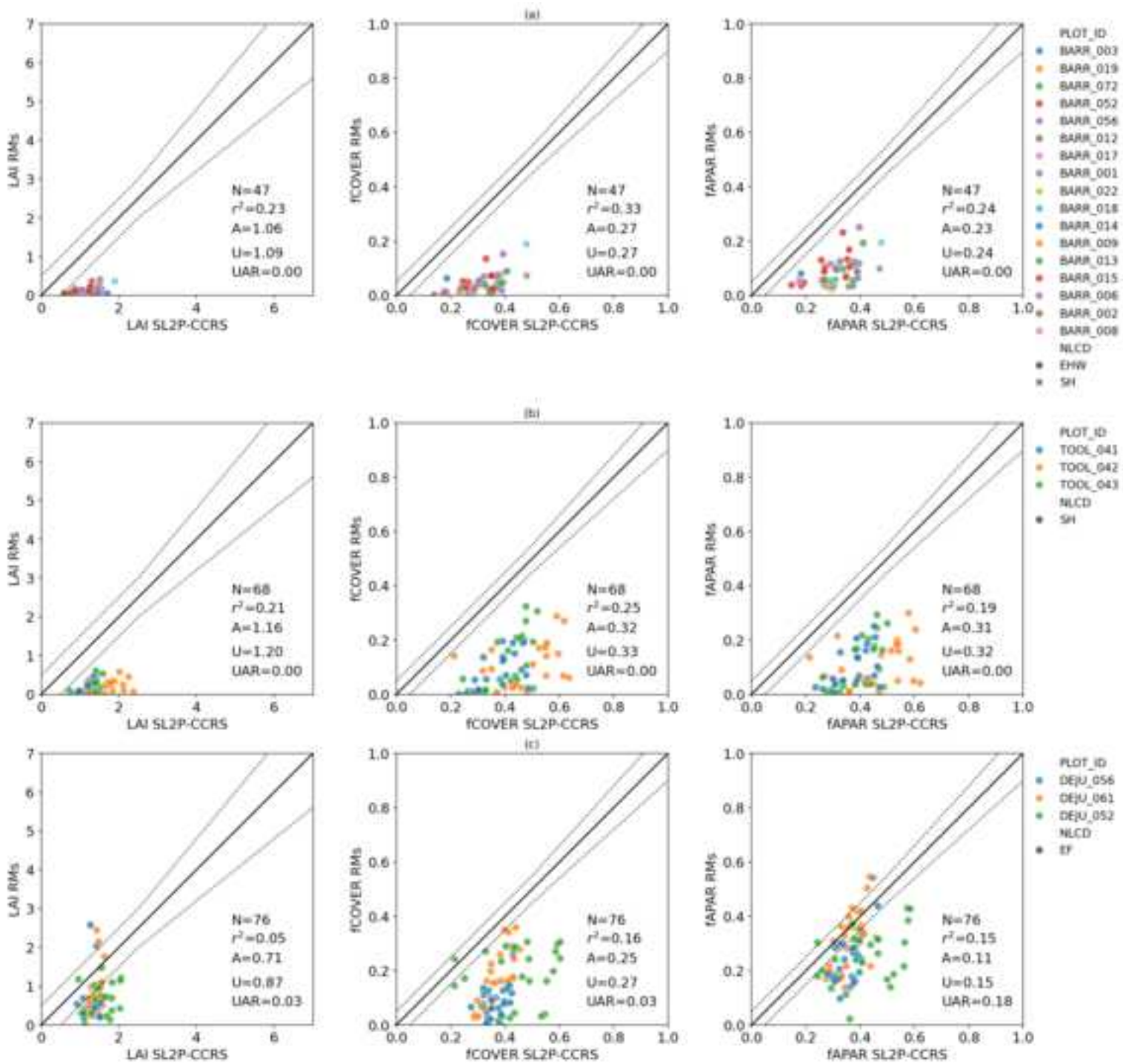
Figure\_9

[Click here to download Figure Figure\\_9.png](#)





Figure\_C1

[Click here to download Figure\\_C1.png](#)


Figure\_E1

[Click here to download Figure\\_E1.png](#)

**Declaration of Interest**

The authors declare that they have no known competing financial interests or personal relationships that could have appeared to influence the work reported in this paper.